Article

Cell Reports

An Oncogenic Role for Alternative NF-κB Signaling in DLBCL Revealed upon Deregulated BCL6 Expression

Graphical Abstract

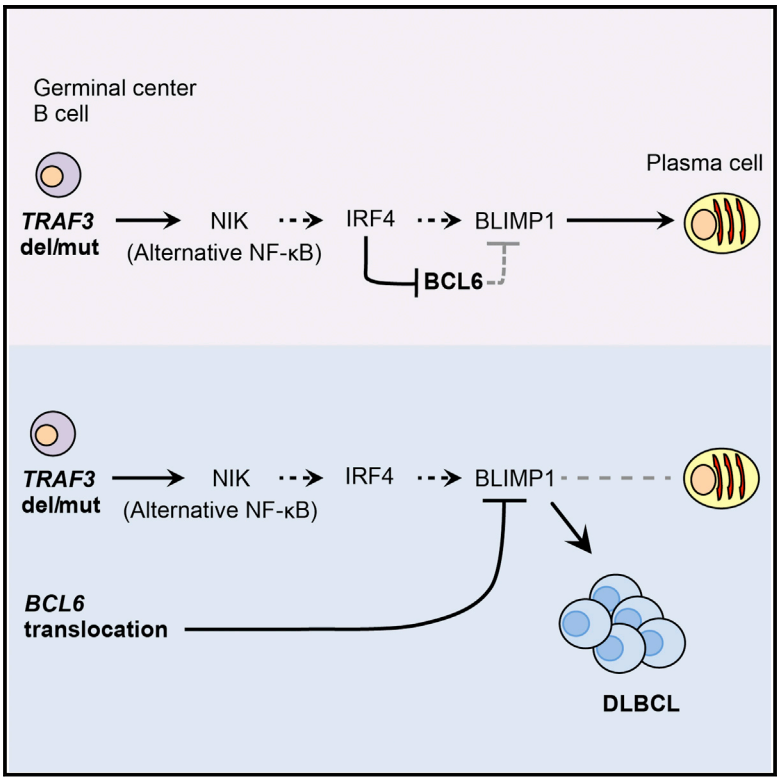

Authors

Baochun Zhang, Dinis Pedro Calado, ..., Laura Pasqualucci, Klaus Rajewsky

Correspondence

baochun_zhang@dfci.harvard.edu (B.Z.), dinis.calado@cancer.org.uk (D.P.C.), klaus.rajewsky@mdc-berlin.de (K.R.)

In Brief

Zhang et al. report that a sizable fraction of human diffuse large B cell lymphomas (DLBCL) carry genetic lesions activating the alternative NF-κB pathway and often accompanied by *BCL6* translocation. Modeling these genetic events in mice, they demonstrate an oncogenic role for the alternative NF-κB pathway in DLBCL pathogenesis.

Highlights

- Genetic loss of *TRAF3* is associated with alternative NF-κB activation in DLBCL
- Constitutive alternative NF-κB activity promotes B cell and plasma cell hyperplasia
- NF-κB-enforced terminal B cell differentiation is repressed by BCL6 in vivo
- Alternative NF-κB signaling cooperates with BCL6 to induce DLBCL in a mouse model

Accession Numbers

GSE65422

Zhang et al., 2015, Cell Reports *11*, 715–726
May 5, 2015
http://dx.doi.org/10.1016/j.celrep.2015.03.059

CellPress

Cell Reports
Article

An Oncogenic Role for Alternative NF-κB Signaling in DLBCL Revealed upon Deregulated BCL6 Expression

Baochun Zhang,[1,2,13,*] Dinis Pedro Calado,[1,3,4,5,13,*] Zhe Wang,[1,2,13] Sebastian Fröhler,[3] Karl Köchert,[3] Yu Qian,[2] Sergei B. Koralov,[1,6] Marc Schmidt-Supprian,[1,7] Yoshiteru Sasaki,[1,8] Christine Unitt,[9] Scott Rodig,[9] Wei Chen,[3] Riccardo Dalla-Favera,[10,11] Frederick W. Alt,[12] Laura Pasqualucci,[10,11,14] and Klaus Rajewsky[1,3,14,*]

[1]Program of Cellular and Molecular Medicine, Children's Hospital, and Immune Disease Institute, Harvard Medical School, Boston, MA 02115, USA
[2]Department of Medical Oncology, Dana-Farber Cancer Institute, Harvard Medical School, Boston, MA 02215, USA
[3]Max Delbrück Center for Molecular Medicine, Robert-Rössle-Str 10, Berlin 13125, Germany
[4]Cancer Research UK, London Research Institute, London WC2A 3LY, UK
[5]Peter Gorer Department of Immunobiology, Kings College London, London SE1 9RT, UK
[6]Department of Pathology, New York University School of Medicine, New York, NY 10016, USA
[7]Department of Hematology and Oncology, Klinikum rechts der Isar, Technische Universität München, Ismaninger Strasse 22, Munich 81675, Germany
[8]Department of Molecular and Cellular Physiology, Graduate School of Medicine, Kyoto University, Kyoto 606-8501, Japan
[9]Department of Pathology, Brigham and Women's Hospital, Boston, MA 02115, USA
[10]Institute for Cancer Genetics and the Herbert Irving Comprehensive Cancer Center, Columbia University, New York, NY 10032, USA
[11]Department of Pathology & Cell Biology, Columbia University, New York, NY 10032, USA
[12]Howard Hughes Medical Institute, Program in Cellular and Molecular Medicine, Boston Children's Hospital, and Department of Genetics, Harvard Medical School, Boston, MA 02115, USA
[13]Co-first author
[14]Co-senior author
*Correspondence: baochun_zhang@dfci.harvard.edu (B.Z.), dinis.calado@cancer.org.uk (D.P.C.), klaus.rajewsky@mdc-berlin.de (K.R.)
http://dx.doi.org/10.1016/j.celrep.2015.03.059

SUMMARY

Diffuse large B cell lymphoma (DLBCL) is a complex disease comprising diverse subtypes and genetic profiles. Possibly because of the prevalence of genetic alterations activating canonical NF-κB activity, a role for oncogenic lesions that activate the alternative NF-κB pathway in DLBCL has remained elusive. Here, we show that deletion/mutation of TRAF3, a negative regulator of the alternative NF-κB pathway, occurs in ~15% of DLBCLs and that it often coexists with *BCL6* translocation, which prevents terminal B cell differentiation. Accordingly, in a mouse model constitutive activation of the alternative NF-κB pathway cooperates with BCL6 deregulation in DLBCL development. This work demonstrates a key oncogenic role for the alternative NF-κB pathway in DLBCL development.

INTRODUCTION

Diffuse large B cell lymphoma (DLBCL), the most common form of non-Hodgkin's lymphoma, is a genetically, phenotypically, and clinically heterogeneous disease. Various DLBCL subtypes have been revealed by gene expression profile analysis using distinct classification schemes, which is according to their putative cell of origin or the coordinated expression of consensus clusters (Alizadeh et al., 2000; Monti et al., 2005). In the "cell of origin" (COO) classification, two main subtypes of DLBCL have been identified in which transcriptional programs resemble normal B cells at particular developmental stages. These are the germinal center B cell (GCB)-like DLBCL, presumably derived from a GC B cell, and the activated B cell (ABC)-like DLBCL, in which the cell of origin is less clear but may correspond to a cell undergoing plasmacytic differentiation (Lenz and Staudt, 2010; Wright et al., 2003).

Analysis of the coding genome of DLBCL has identified various genetic lesions and revealed their association with the GCB or ABC subtype. Inactivating mutations and deletions of *BLIMP1*/*PRDM1*, a key gene in terminal B cell differentiation, are found exclusively in the ABC subtype (~30% of cases) (Mandelbaum et al., 2010; Pasqualucci et al., 2006; Tam et al., 2006). Similarly BCL6 expression is deregulated by chromosomal translocation more frequently in the ABC (~26% of cases) than in the GCB subtype, where BCL6 expression is high a priori (Iqbal et al., 2007; Mandelbaum et al., 2010; Pasqualucci et al., 2011). Interestingly, *BCL6* translocations are mutually exclusive with *BLIMP1* structural alterations in ABC-DLBCL (Mandelbaum et al., 2010). Given that BCL6 can directly suppress BLIMP1 expression (Tunyaplin et al., 2004), it has been hypothesized that *BCL6* translocations represent an alternative mechanism for BLIMP1 inactivation in ABC-DLBCL, although BCL6 controls multiple additional functions in GC B cells (Mandelbaum et al., 2010). Another group of mutations promote constitutive NF-κB

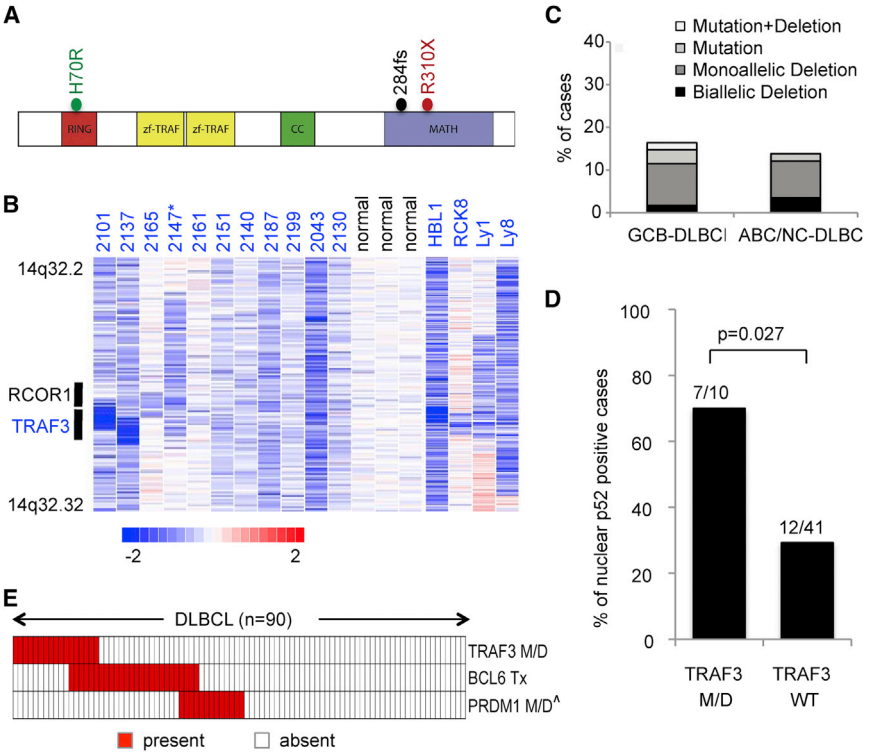

Figure 1. Recurrent *TRAF3* and *BCL6* Lesions in DLBCL

(A) Diagram of the TRAF3 protein, with its relevant functional domains. The mutations found in DLBCL are indicated.

(B) Inferred log2 copy-number (CN) data from representative DLBCL cases carrying deletions encompassing *TRAF3* compared with normal controls. The position of *TRAF3* and its neighboring gene *RCOR1* is indicated. In the red-blue scale, white corresponds to a normal (diploid) CN log ratio; blue is deletion, and red is gain. *Case 2147 harbored a point mutation in the residual allele, leading to biallelic inactivation.

(C) Overall frequency of *TRAF3* genetic lesions (point mutations and deletions) in DLBCL phenotypic subtypes. Forty-seven GCB and 51 ABC/NC-DLBCL biopsies, 14 GCB and 7 ABC-DLBCL cell lines were included in this analysis (the primary tumors and cell lines of each DLBCL subtype displayed similar frequencies of *TRAF3* lesions). Note that among the 119 samples, 29 lack CN data; thus, the frequencies shown may represent an underestimate.

(D) Percentage of DLBCL primary cases showing nuclear p52 staining, as a readout of noncanonical NF-κB activation, in TRAF3 M/D versus TRAF3 WT cases. The cutoff used to score cases as nuclear positive was ≥20% (Compagno et al., 2009).

(E) Relative distribution of genetic lesions affecting *TRAF3*, *BCL6*, and *PRDM1* in individual DLBCLs. Each column represents one patient, with color codes indicating the presence or absence of the corresponding feature (Tx, translocation; M/D, mutations and/or deletions). Only the 90 samples with full information on *TRAF3* M/D, *BCL6* Tx, and *PRDM1* M/D are included. ^*PRDM1* genetic lesions only include biallelic deletions or point mutations since the functional significance of large 6q monoallelic deletions is unclear. Details of *PRDM1* and *BCL6* lesions have been described previously (Mandelbaum et al., 2010; Pasqualucci et al., 2006).

See also Figure S1.

activation, such as those affecting *TNFAIP3* (*A20*), *CD79B*, and *MYD88*, predominantly in the ABC subtype (Compagno et al., 2009; Davis et al., 2010; Ngo et al., 2011; Pasqualucci et al., 2011), and *CARD11* mutations occurring in both subtypes (Lenz et al., 2008; Pasqualucci et al., 2011).

Notably, NF-κB activating mutations in DLBCLs, including the ones described above, predominantly involve the NF-κB canonical pathway (Compagno et al., 2009; Davis et al., 2010; Lenz et al., 2008; Ngo et al., 2011; Pasqualucci et al., 2011; Staudt, 2010). As a consequence, a role for putative genetic lesions involving the NF-κB alternative pathway remained largely overlooked. Supporting a role of the NF-κB alternative pathway in DLBCL pathogenesis, ~10% of DLBCLs were found to stain positive for NF-κB2 p52 but not NF-κB1 p50 in the nucleus, and another 20% of cases exhibited both NF-κB1 and NF-κB2 nuclear staining (Compagno et al., 2009); furthermore, a recent study revealed that roughly 10% of DLBCLs carry deletions or mutations of *TRAF3* or *TRAF2* (Pasqualucci et al., 2011). TRAF3 and TRAF2 control the degradation of NF-κB-inducing kinase (NIK) and consequently restrain activation of the alternative NF-κB pathway (Gardam et al., 2008; Häcker et al., 2011; Sasaki et al., 2008).

Although an oncogenic role for constitutive canonical NF-κB activity has been demonstrated in a mouse model of DLBCL (Calado et al., 2010), a functional link between the activation of alternative NF-κB pathway and the pathogenesis of DLBCL remained to be established. In this study, we performed complementary human and mouse studies to investigate mutations activating the alternative NF-κB pathway and concurrent genetic events and developed a genetic system in the mouse to test the role of constitutive alternative NF-κB signaling in the pathogenesis of DLBCL.

RESULTS

TRAF3 Gene Lesions Coexist with *BCL6* Translocation in Human DLBCL

Deletions and mutations of *TRAF3* have been found in human DLBCLs (Pasqualucci et al., 2011). To have a deeper look into *TRAF3* genetic lesions and their distribution in DLBCL subtypes, we analyzed the *TRAF3* sequences for the presence of point mutations and copy-number aberrations in 119 DLBCL samples, including 98 biopsies and 21 cell lines whose phenotypic subtype was known. This analysis revealed missense, frameshift, and nonsense mutations (the two mutations tested being both somatic in origin) in functional domains, which are required for TRAF3 to negatively regulate NIK protein stability (Figure 1A; Annunziata et al., 2007; Häcker et al., 2011; He et al., 2007; Keats et al., 2007). Specifically, we identified one DLBCL case carrying a frameshift mutation (284 fs) and one carrying a nonsense

mutation (R310X), both of which are predicted to disrupt the MATH domain, required for the interaction between TRAF3 and NIK (Häcker et al., 2011; He et al., 2007). One additional DLBCL harbored a missense mutation (H70R) that may alter the function of the RING domain, required for the negative regulation of NIK by TRAF3 (He et al., 2007). Notably, a missense mutation affecting the H70 residue has been previously reported in a multiple myeloma patient (Keats et al., 2007). The present analysis also identified biallelic or monoallelic deletions involving the *TRAF3* locus, including two focal homozygous losses that encompass *TRAF3* and its neighboring gene *RCOR1* (Figure 1B). A similar spectrum of deletions has been observed in human multiple myeloma and was shown to stabilize the NIK protein (Annunziata et al., 2007; Keats et al., 2007). *TRAF3* deletions/mutations occurred similarly in GCB and ABC DLBCL (Figure 1C) and significantly correlated with alternative NF-κB activation, indicated by nuclear p52 staining (Figure 1D).

We previously observed that constitutive canonical NF-κB activation promotes DLBCL development upon disruption of terminal B cell differentiation via inactivating BLIMP1 (Calado et al., 2010). With these observations in mind, we searched whether TRAF3 mutations in DLBCL associate with BCL6 or BLIMP1 genetic lesions, either of which would presumably disrupt terminal B cell differentiation (Mandelbaum et al., 2010). While none of the 17 DLBCLs carrying *TRAF3* deletions/mutations exhibited biallelic *BLIMP1* deletion/mutation, 6 of them (35%) had concurrent *BCL6* translocation (the small number of cases analyzed did not provide statistical power to assess whether the co-occurrence is significant) (Figures 1E and S1).

Taken together, these data show that roughly 15% of DLBCLs carry *TRAF3* genetic alterations and that these lesions often coexist with *BCL6* translocations.

Impact of Alternative NF-κB Activation and/or BCL6 Deregulation on the GC Reaction

To study the impact of enforced alternative NF-κB activation and BCL6 deregulation on the pathogenesis of DLBCL, we used a system of conditional gain- and/or loss-of-function mutagenesis in mice. Given that DLBCL arises from a GC or post-GC B cell (Shaffer et al., 2012), we decided to perform targeted mutagenesis in GC B cells, using the *Cγ1-cre* transgene, from which Cre is expressed in B cells at an early stage of the GC reaction (Casola et al., 2006). To induce activation of the alternative NF-κB pathway, we combined this transgene with a *ROSA26* allele harboring a cDNA encoding NIK, preceded by a *loxP* flanked *STOP* cassette (hereafter called Nik^{stopFL}) (Sasaki et al., 2008). NIK expression from the mutant ROSA26 allele is indicated by a GFP reporter controlled by an internal ribosome entry site (Sasaki et al., 2008). For BCL6 deregulated expression, we used an HA-tagged *BCL6* transgene inserted into the immunoglobulin (Ig) heavy-chain locus downstream of Iμ promoter (hereafter called *IμBcl6*), mimicking the observed *BCL6*/*IgH* translocation in DLBCL (Cattoretti et al., 2005). To monitor Cre-mediated recombination in cells of compound mutant mice not carrying the Nik^{stopFL} allele, we used a conditional YFP reporter allele in the ROSA26 locus designated YFP^{stopFL} (Srinivas et al., 2001). Mice carrying the *Cγ1-cre* and YFP^{stopFL} alleles served as controls.

To test the impact of alternative NF-κB pathway activation, alone or together with enforced BCL6 expression, on GC B cell formation, we immunized experimental and control mice with sheep red blood cells (SRBCs). Analysis 10 days after immunization revealed expression of the reporter, GFP or YFP, in the majority of GC B cells, indicating efficient Cre-mediated recombination in mice of all genotypes analyzed (Figure 2A). Control mice and mice with enforced expression of NIK and/or BCL6 also showed similar fractions of GC B cells at day 10 after primary immunization (Figures 2A and 2C). However, at day 21 postimmunization, mice with enforced NIK expression and thus constitutive alternative NF-κB activation alone had a significantly reduced fraction of GC B cells compared with control mice (Figures 2B and 2C), similar to what is seen in mice with constitutive canonical NF-κB activation in GC B cells (Calado et al., 2010). Enforced NIK expression in GC B cells led to increased expression of *IRF4*, which might, in turn, account for upregulation of *BLIMP1* and downregulation of *BCL6* in these cells (Figure 2D; Saito et al., 2007; Sciammas et al., 2006). We considered the possibility that the premature termination of the GC reaction in mice with enforced NIK expression might be due to the altered expression of BLIMP1 or BCL6 (Calado et al., 2010; Martins and Calame, 2008; Ye et al., 1997); however, concomitant *BLIMP1* deletion (data not shown) or BCL6 enforced expression did not prevent GC early termination in these mice (Figures 2B and 2C). We next looked whether activation of the alternative NF-κB pathway alone or together with enforced BCL6 expression affects physiological processes of GC B cells, such as somatic hypermutation. At day 21 postimmunization, GC B cells from mice with enforced NIK or BCL6 expression alone carried slightly reduced numbers of somatic mutations in their Ig heavy-chain (IgH) V regions, compared with controls, while those from mice with enforced expression of both NIK and BCL6 had significantly fewer mutations (Figure 2E). The reduced somatic mutation load in the latter group is likely due to premature termination of the GC reaction, as similar levels of somatic mutation and *AICDA* expression were detected in GC B cells from these mice and controls when analyzed at day 10 after immunization, the peak time of the GC reaction (Figures 2C, 2E, and 2F). Collectively, these results demonstrate that constitutive activation of NF-κB signaling through enforced NIK expression negatively impacts the GC reaction and that this effect is independent of BCL6 regulation. Hence, constitutive NF-κB activation is incompatible with the maintenance of a GC B cell phenotype and may in a similar way impact the phenotype of lymphoma cells arising in the context of the GC reaction (see Discussion).

Enforced Activity of the Alternative NF-κB Pathway Enhances B Cell Proliferation and Survival

To evaluate the impact of the constitutive expression of NIK and/or BCL6 on B cell proliferation and survival, we used an in vitro cell culture system where Cre-mediated recombination is induced in B cells upon treatment with anti-CD40 and interleukin 4 (IL-4), mimicking T cell-dependent B cell activation (Calado et al., 2010). NF-κB activation through enforced expression of NIK not only improved survival of ABCs but also increased their proliferation (Figures 3A–3C). Interestingly, in

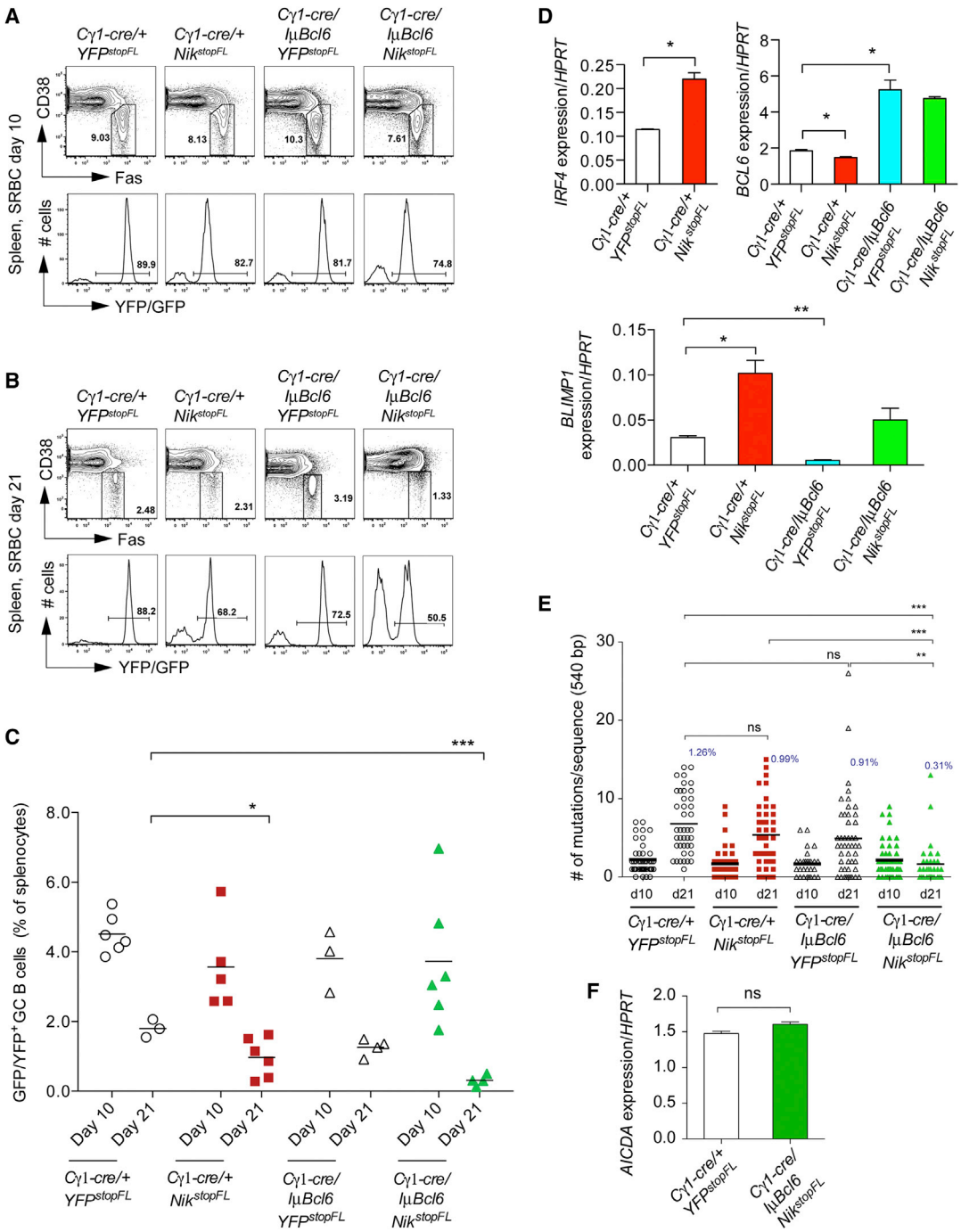

Figure 2. Impact of Constitutive NIK and BCL6 Expression on the GC Reaction

(A and B) Representative FACS analysis of splenic GC B cells at day 10 (A) and day 21 (B) after primary immunization with SRBCs, respectively. (Upper) The GC B cell population (within the gate; $CD19^{+}Fas^{hi}CD38^{lo}$). (Lower) Reporter expression in GC B cells.

(C) Summary of FACS analysis of GC B cells as in (A) and (B). Black bar represents mean for each genotype of mice at the indicated time points.

(D) Real-time PCR analysis of the expression levels of the indicated genes in reporter-positive GC B cells at day 10 after primary immunization with SRBCs. Values represent normalized levels to *HPRT*. Data are represented as mean ± SEM.

(E) *IgH* somatic mutation in reporter-positive GC B cells at day 10 (13 to 16 sequences per mouse from two to three mice per genotype) and day 21 (12–16 sequences per mouse from two to three mice per genotype) after primary immunization with SRBCs. Black bar represents mean. Average mutation frequency at day 21 is shown in graph.

(F) Real-time PCR analysis of *AICDA* transcript levels in reporter-positive GC B cells at day 10 after primary immunization with SRBCs. Values represent normalized levels to *HPRT*. Data are represented as mean ± SEM.

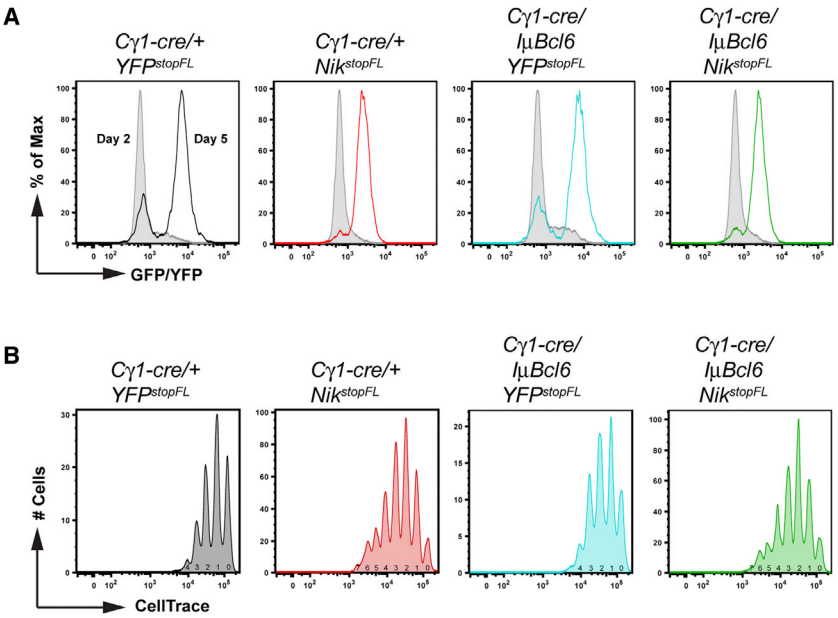

Figure 3. Enhanced Cellular Proliferation and Survival as a Result of Constitutive NIK Expression

(A) Cre-mediated recombination efficiency in purified B cells from mice of the indicated genotypes, cultured in vitro in the presence of anti-CD40 plus IL-4, measured by expression of reporter genes at days 2 and 5 of the culture.

(B) Proliferation of in vitro cultured B cells treated as in (A), measured by CellTrace dilution of reporter-positive cells at day 5 of the culture. The numbers under CellTrace peaks indicate the number of cell divisions.

(C) Frequency of apoptotic cells, at day 5, within in vitro cultured B cells treated as in (A), measured by active Caspase3 staining.

(D) Relative number of live cells at the indicated time points in in vitro culture of splenic B cells treated as in (A), normalized to day 2.

Data in (A–D) are representative of two independent experiments performed in triplicate; data in (C) are shown as mean ± SEM of triplicates; data in (D) are shown as mean ± SD of triplicates.

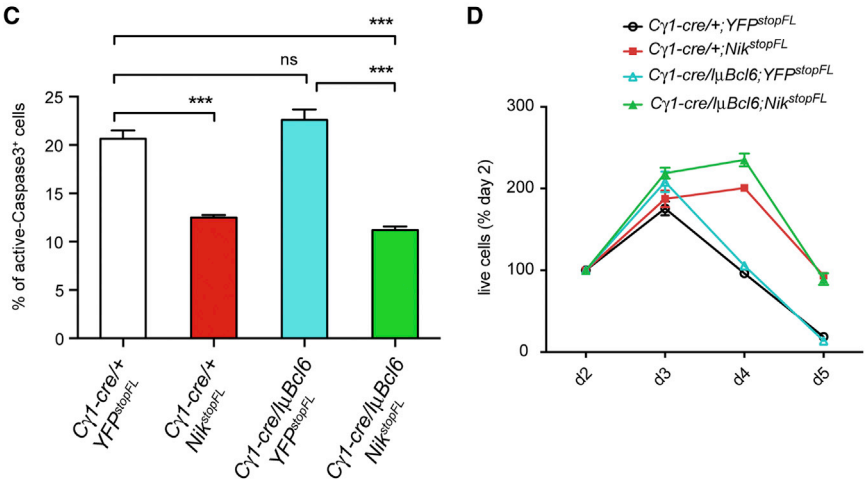

this experimental system, concurrent BCL6 expression did not further enhance these effects (Figures 3A–3C). Overall, constitutive NIK expression led to the accumulation of increased numbers of cells in culture, with concomitant BCL6 expression having no additional effect (Figure 3D).

BCL6 Enforced Expression through a *BCL6/IgH* Translocation Blocks Plasma Cell Differentiation Induced by Constitutive Alternative NF-κB Signaling

Enforced expression of NIK in GC B cells promoted transcription of *IRF4* (Figure 2D), a key transcription factor for plasma cell differentiation (Klein et al., 2006). Accordingly, SRBC-immunized *Cγ1-cre/+;Nik*^{stopFL} mice displayed a significantly enlarged plasma cell compartment after primary and secondary immunization compared with controls (Figures 4A, 4B, and S2A). In accord with the notion that BCL6 represses *BLIMP1* transcription (Figure 2D; Tunyaplin et al., 2004) and the latter is essential for plasma cell differentiation (Martins and Calame, 2008), the plasma cell compartment was significantly reduced in *Cγ1-cre/IμBcl6;Nik*^{stopFL} mice compared with *Cγ1-cre/+;Nik*^{stopFL} mice (Figures 4A, 4B, and S2A). In line with the in vitro data that enforced alternative NF-κB activity enhances B cell proliferation and survival, while concurrent BCL6 expression has no additive effect (Figure 3), *Cγ1-cre/+;Nik*^{stopFL} mice displayed increased numbers of total reporter positive cells (containing both plasma cells and B cells) in spleen compared to controls (*Cγ1-cre/+;YFP*^{stopFL}), and these numbers were not further increased in mice with concurrently enforced expression of BCL6 (*Cγ1-cre/IμBcl6;Nik*^{stopFL} mice) (Figures 4A and S2B). Collectively, these data suggest that a major effect of the deregulated BCL6 expression in GC B cells is a block of plasma cell differentiation.

Mice with Enforced NIK and BCL6 Expression in GC B Cells Display a Shortened Lifespan

Next, we assessed the role of alternative NF-κB activation with or without concomitant BCL6 deregulation in B cell malignant transformation by monitoring the mice for tumor development over a period of 1.5 years (78 weeks). Mice with enforced expression of NIK displayed a similar lifespan as controls, while ~40% of *Cγ1-cre/IμBcl6* mice died prematurely (Figure 5), consistent with a previous report (Cattoretti et al., 2005). In contrast, all mice with concurrent NIK and BCL6 enforced expression died within the observation period, suggesting a cooperative role (Figure 5).

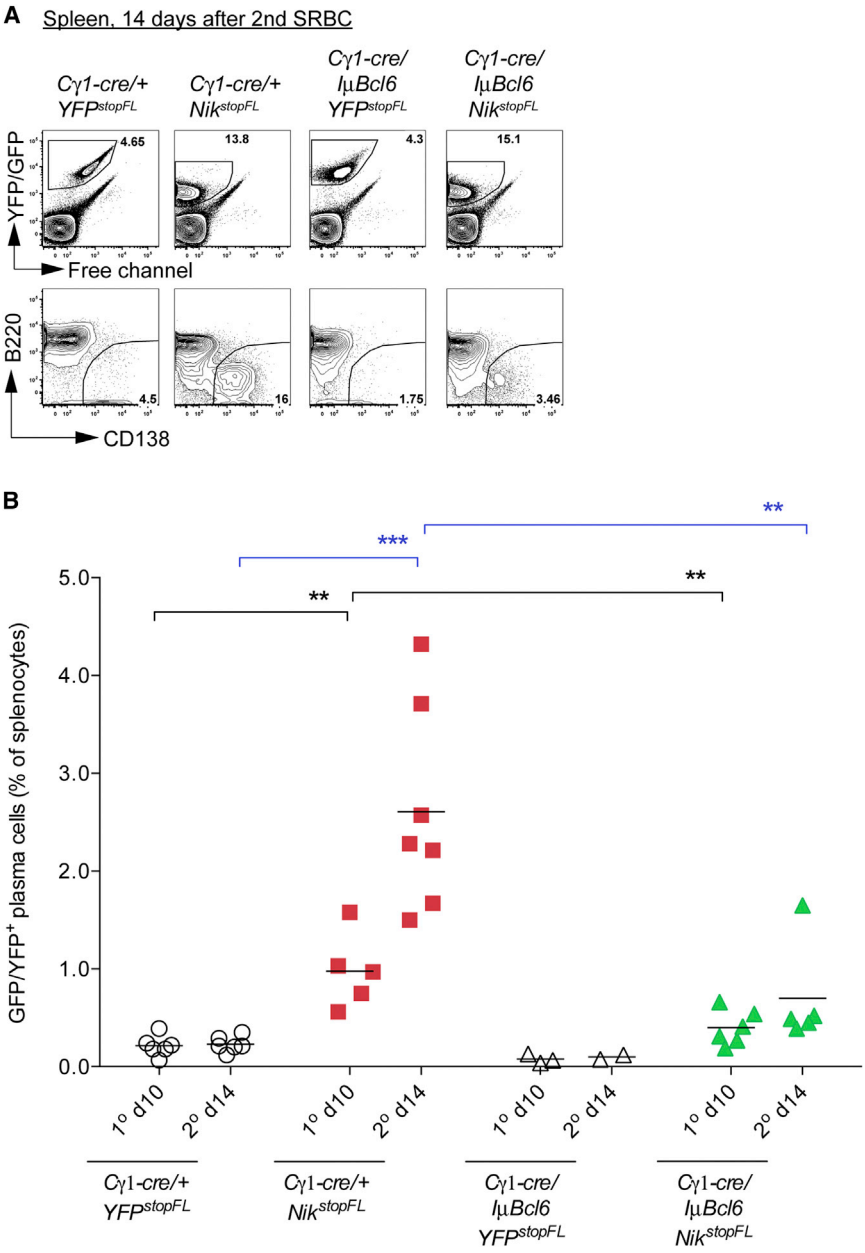

Figure 4. Plasma Cell Differentiation Induced by NIK Expression Is Largely Abolished upon Coexpression of BCL6

(A) Representative FACS analysis of plasma cells in spleen at day 14 after secondary immunization. Reporter-positive splenic cells from mice of the indicated genotypes were gated (upper) for the analysis of plasma cells ($B220^{lo}CD138^{+}$; lower).

(B) Summary of FACS analysis of plasma cells in spleen at day 10 after primary immunization and day 14 after secondary immunization. Black bar represents mean.

See also Figure S2.

Plasma Cell Hyperplasia in Mice with Constitutive Alternative NF-κB Signaling

We decided to analyze the *Cγ1-cre/+;Nik*^{stopFL} mice in more detail and sacrificed them at the end of the observation period (1.5 years). Mice with enforced NIK expression displayed enlarged spleens (Figure 6A) and had a significant hyperplasia of both B cells and plasmablasts/plasma cells in spleen and bone marrow compared with age-matched control animals (Figures 6B and S3). Histological analysis revealed dramatically increased numbers of spleen cells expressing the plasma cell marker CD138 and intracellular Ig (Figure 6C). Serum protein electrophoresis further revealed that 8/9 of *Cγ1-cre/+;Nik*^{stopFL} mice displayed a distinct band in the γ-globulin region of the gel (M-spike), in contrast to three of nine of controls (Figure 6D; data not shown), indicative of clonal plasma cell expansion. We conclude that enforced activation of alternative NF-κB signaling promotes B cell hyperplasia, in accord with previous work (Sasaki et al., 2008), as well as an expansion of the plasma cell compartments in spleen and bone marrow.

Alternative NF-κB Signaling Cooperates with Deregulated BCL6 in DLBCL Pathogenesis

Macroscopic examination of terminally ill *Cγ1-cre/IμBcl6* (6 cases) and *Cγ1-cre/IμBcl6;Nik*^{stopFL} (10 cases) mice revealed splenomegaly and lymphadenopathy in all cases (Figure 7A). Histological examination of the enlarged lymphoid organs showed that five of the six *Cγ1-cre/IμBcl6* mice analyzed had a DLBCL-like disease, characterized by a diffuse growth pattern of large cells, while the remaining mouse had a tumor with a plasmacytic morphology. Diseased *Cγ1-cre/IμBcl6;Nik*^{stopFL} mice on the other hand all showed histological features of DLBCL (Figure 7B; Table S1; data not shown). By flow cytometry, these tumors were all negative for the plasma cell marker CD138 and displayed a mature B cell phenotype ($CD19^{+}AA4.1^{-}IgM^{+}$ or occasionally IgG^{+}; Table S2). Analysis of IgH gene rearrangements by Southern blot revealed that the DLBCLs were of clonal B cell origin and that the same tumor clone was present in both spleen and mesenteric lymph nodes of each mouse examined (Figure 7C), indicative of an aggressive phenotype. We next amplified the rearranged IgH V regions from clonal B cell tumors of *Cγ1-cre/IμBcl6* and *Cγ1-cre/IμBcl6;Nik*^{stopFL} mice (four cases each). Sequence analysis revealed somatically mutated Ig genes in three of the four *Cγ1-cre/IμBcl6* tumors and two of the four *Cγ1-cre/IμBcl6;Nik*^{stopFL} tumors (Table S3), suggesting that a fraction of the tumors derived from GC or post-GC B cells.

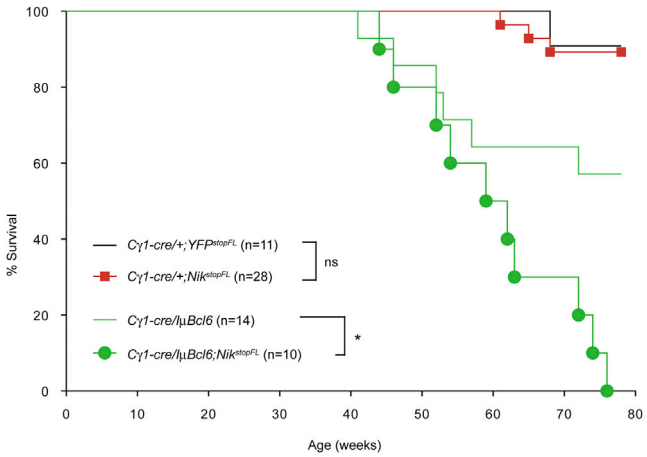

Figure 5. Mice with Enforced NIK and BCL6 Expression Display a Shortened Lifespan

Kaplan-Meier survival curves of mice of the indicated genotypes.

The activation of the alternative NF-κB pathway was confirmed in all tumors from *Cγ1-cre/IμBcl6;Nik*^{stopFL} mice by the enhanced processing of p100 to p52 on the immunoblot compared with tumors from *Cγ1-cre/IμBcl6* mice (Figure 7D).

In an attempt to subclassify the lymphomas occurring in our mouse cohorts according to the COO classification scheme, we performed immunohistochemistry (IHC) and gene expression profiling (GEP) by RNA sequencing (RNA-seq). By IHC, expression of IRF4/MUM1 usually segregates with ABC-DLBCL, while high levels of BCL6 expression often associate with GCB-DLBCL (Choi et al., 2009; Hans et al., 2004), although a fraction of ABC-DLBCLs also expresses BCL6 in part due to *BCL6* translocation to the *IgH* locus (Iqbal et al., 2007; Lenz and Staudt, 2010). All tumors analyzed were BCL6 positive, in line with the presence of the *IμBcl6* allele mimicking the *BCL6/IgH* chromosomal translocation (Figure 7E; Table S1). However, the expression was varied and particularly low in the cases where NIK expression was enforced (Figures 7D and 7E; Table S1). These observations suggest that the alternative NF-κB pathway was able to inhibit BCL6 expression from its endogenous loci, but not from the transgene, similar to what had been observed for the canonical pathway (Figure 2D; Cattoretti et al., 2005; Saito et al., 2007). IHC for IRF4, on the other hand, revealed that all lymphomas (five of five) arising in *Cγ1-cre/IμBcl6;Nik*^{stopFL} mice were IRF4^{hi}, while a more varied pattern was observed in tumors arising in *Cγ1-cre/IμBcl6* mice, with two IRF4^{hi} tumors, one tumor displaying both IRF4^{dim} and IRF4^{hi} cells and one IRF4$^{lo/neg}$ tumor (Figure 7E; Table S1). To subclassify these DLBCLs, we compared their GEP to that of GC B cells and in vitro ABCs, in analogy to the strategy used for classification of human DLBCLs (Alizadeh et al., 2000). This analysis revealed that three (#603, #604, #775) of five DLBCLs arising in *Cγ1-cre/IμBcl6* mice displayed a GEP similar to GC B cells, indicative of the GCB subtype, while the GEP of the remaining two (#607, #1128) *Cγ1-cre/IμBcl6* lymphomas resembled that of ABCs. Of note, tumors #607 and #1,128 were also IRF4^{hi} by IHC, further supporting an ABC subtype classification. In contrast, most DLBCLs (six of seven; #817, #773, #920, #776, #611, #1,078) occurring upon activation of the alternative NF-κB pathway together with enforced BCL6 expression (*Cγ1-cre/IμBcl6;Nik*^{stopFL} mice) displayed a GEP similar to that of ABCs (Figure 7F). The remaining *Cγ1-cre/IμBcl6;Nik*^{stopFL} DLBCL (#818) had a GEP resembling that of GC B cells, but because it stained highly positive for IRF4, we considered it "nonclassified." Thus, in our experimental system, the alternative NF-κB pathway and BCL6 synergize in the development of lymphomas that, in most cases, resemble ABC-DLBCL.

Mutations in Genes of the Canonical NF-κB Pathway in a Fraction of Mouse DLBCLs

Our genetic analysis revealed that a fraction (6 of 17) of human DLBCLs carrying a mutated TRAF3 gene have an additional mutation(s) in genes of the canonical NF-κB pathway (Figure S1). In the tumors of *Cγ1-cre/IμBcl6;Nik*^{stopFL} mice we detected variable levels of phospho-IκBα at Ser32/26 (Figure 7D). Phosphorylation at these residues indicates canonical NF-κB activation (Brown et al., 1995; Traenckner et al., 1995). For that reason we decided to analyze the RNA-seq data of the DLBCLs arising in the compound mutant mice for acquired mutations affecting genes within the canonical NF-κB pathway (for the list of genes, see Supplemental Experimental Procedures). Interestingly, we found such mutations in two of seven DLBCLs arising in *Cγ1-cre/IμBcl6;Nik*^{stopFL} mice (Figure S4). More specifically, DLBCLs #773 and #776 harbored the same mutation (R218H) in the MYD88 gene, and increased levels of phospho-IκBα were seen in DLBCL #773 compared with other tumors of the same genotype and normal splenic tissue from a *Cγ1-cre/+* mouse (Figure 7D), suggesting a functional role for this mutation (Ngo et al., 2011). We also analyzed RNA-seq data of the DLBCLs arising in mice with enforced BCL6 expression alone for the presence of mutations in genes of both canonical and alternative pathways of NF-κB (for the list of genes, see the Supplemental Experimental Procedures). We found that two of five such DLBCLs had acquired mutations in either the CK1α kinase or CARD11 gene (Figure S4; Bidère et al., 2009; Lenz et al., 2008). DLBCL #1,128 had a mutation in the CK1α kinase domain and displayed elevated phospho-IκBα compared with the normal spleen control (Figure 7D). These observations are consistent with the observed IRF4 expression in this tumor and classification as ABC-DLBCL (Figure 7F). Another *Cγ1-cre/IμBcl6* derived DLBCL (#603) displayed a mutation in the CARD11 (D401N) coiled-coil domain, to which the CARD11 mutations in human DLBCL are confined (Lenz et al., 2008), and this lymphoma also showed elevated levels of phospho-IκBα compared with the normal spleen control (Figure 7D). Despite canonical NF-κB pathway activation, this tumor was classified as a GCB-DLBCL by GEP profiling. Interestingly, the same exact mutation has been found in a human GCB-DLBCL (Morin et al., 2011). This is consistent with previous observations in human DLBCL, where canonical NF-κB activation could be detected in ~20% of GCB-DLBCLs (Compagno et al., 2009). Collectively, our data show that a fraction of the tumors arising in both *Cγ1-cre/IμBcl6* and *Cγ1-cre/IμBcl6;Nik*^{stopFL} mice has acquired mutations in genes of the canonical NF-κB pathway

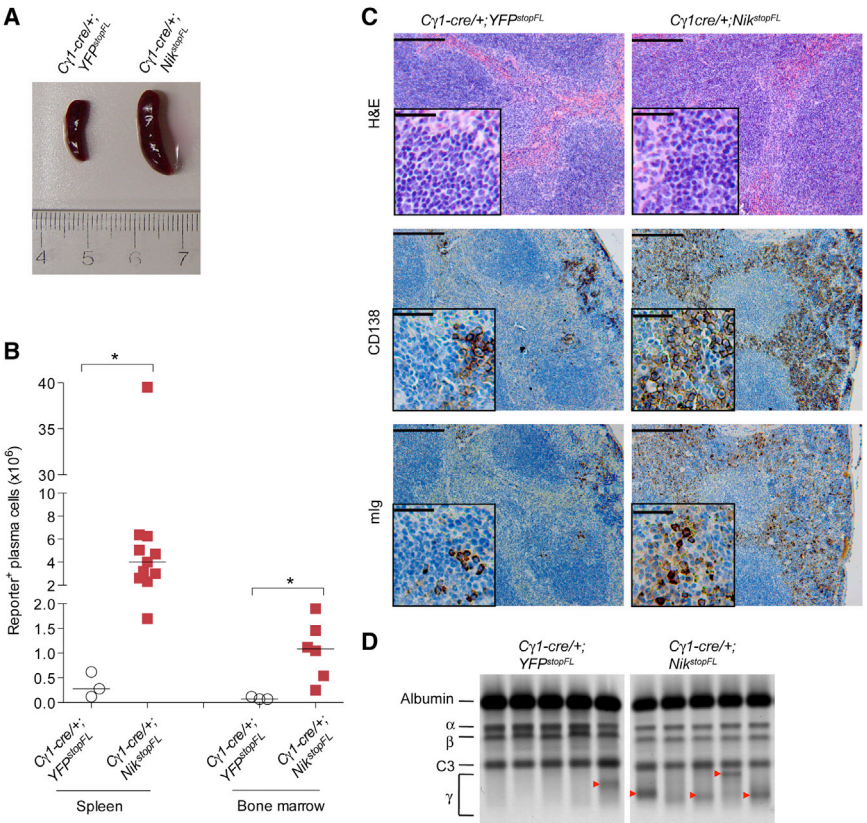

Figure 6. Plasma Cell Hyperplasia in Mice with Constitutive Alternative NF-κB Signaling

(A) Representative picture of spleens from aged mice (≥60 weeks) of the indicated genotypes. Three or more mice per genotype were analyzed.

(B) Number of reporter-positive plasma cells ($B220^{lo}CD138^{+}$) in spleen and bone marrow of aged mice of the indicated genotypes. Black bar represents median. The statistics was analyzed using unpaired, nonparametric Mann-Whitney test (comparing ranks).

(C) Representative histological (H&E) and immunohistochemical (CD138 and Ig) staining of spleens from aged mice of the indicated genotypes. Three or more mice per genotype were analyzed. Scale bar represents 1,000 μm; inset represents 200 μm.

(D) Serum protein electrophoresis of representative samples from aged mice of the indicated genotypes. The position of albumin and of various globulin components of the serum is indicated. Red arrowhead indicates M spike. In total, three of nine (33%) of *Cγ1-cre/+;YFP*^{stopFL} mice and eight of nine (89%) of *Cγ1-cre/+;Nik*^{stopFL} mice display M spike, respectively.

See also Figure S3.

that are also affected in human DLBCL (Compagno et al., 2009; Pasqualucci et al., 2011).

DISCUSSION

A Causal Role of Alternative NF-κB Activation in DLBCL

Recent studies of human DLBCLs have identified various genetic lesions that activate NF-κB through the canonical pathway and revealed their association predominantly with the ABC over the GCB subtype (Compagno et al., 2009; Davis et al., 2010; Kato et al., 2009; Lenz et al., 2008; Ngo et al., 2011; Pasqualucci et al., 2011), in accord with the observation that ABC-DLBCL but not GCB-DLBCL cell lines rely on constitutive canonical NF-κB signaling for survival (Davis et al., 2001; Staudt, 2010). Using a mouse model, we had previously established an oncogenic role for constitutive canonical NF-κB activity in ABC-DLBCL pathogenesis (Calado et al., 2010). In contrast, the question of whether enforced activation of the alternative NF-κB pathway can be functionally involved in DLBCL pathogenesis has not been addressed, despite several observations suggesting a role for this pathway in the disease. Thus, mutations affecting genes (*TRAF3* and *TRAF2*) of the alternative NF-κB pathway have been observed in a subset of human DLBCLs (Pasqualucci et al., 2011); the NF-κB2 gene, encoding the core molecule for this signaling pathway, was originally identified by virtue of its translocation to the IgH locus in a case of DLBCL (Neri et al., 1991), and IHC data revealed nuclear NF-κB2 p52, reflecting activation of the alternative pathway, in a subset of both GCB and ABC-DLBCL (Compagno et al., 2009). While these data demonstrated alternative NF-κB activity in a subset of DLBCLs, a paper by Pham et al. (2011) claimed that in DLBCLs of all subtypes both the canonical and alternative NF-κB pathways are activated through constitutive BAFF-R (BR3) signaling. However, in most DLBCL cell lines analyzed, there was no evidence for robust degradation of p100 to p52.

To clarify these matters and in particular to obtain functional evidence for a contribution of alternative NF-κB signaling to DLBCL pathogenesis, we first extended the analysis of *TRAF3* mutations by studying a larger number of DLBCL primary tumors and examining the association of *TRAF3* mutations with the ABC or GCB subtype. These analyses demonstrated that biallelic or monoallelic deletions/mutations of *TRAF3* occur recurrently in similar fractions (~15%) of ABC-DLBCL and GCB-DLBCL and correlate with alternative NF-κB activity in these cases. We then developed a mouse model system that allows conditional activation of the alternative NF-κB pathway in a GC B-cell-restricted manner and found that activation of this pathway, in concert with BCL6 deregulation, leads to the development of DLBCL. This indicates a causal role of deregulated alternative NF-κB signaling in DLBCL pathogenesis. Interestingly, in this scenario, the deregulation of alternative NF-κB activity appears to be required in the context of GC B cell differentiation. Deletion of *TRAF3* in mouse B cells from early developmental stages via *CD19-cre* leads to the formation of B1 and marginal zone B cell lymphomas, not DLBCL (Moore et al., 2012). These tumors resemble human splenic marginal zone lymphoma (SMZL), where inactivating mutations of *TRAF3* have also been found

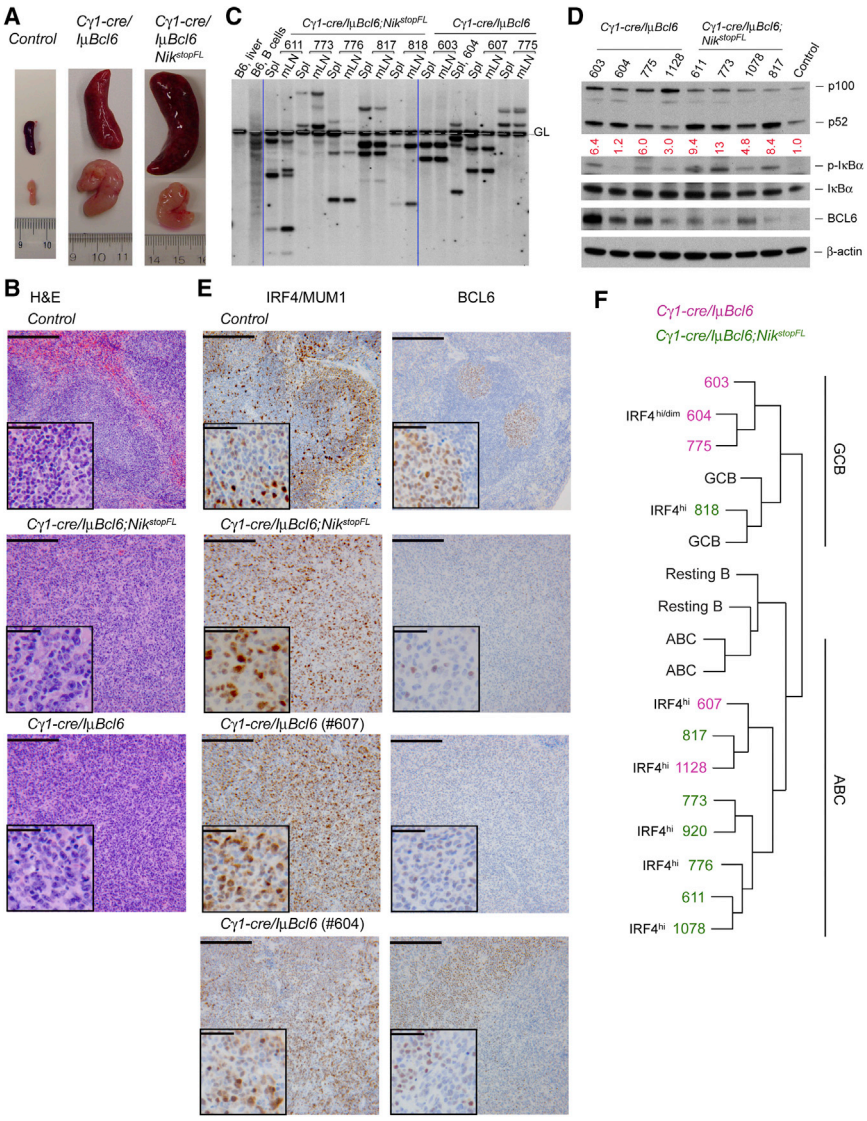

Figure 7. Constitutive Alternative NF-κB Activation Synergizes with BCL6 in DLBCL Formation and Progression

(A) Representative pictures of spleens and mesenteric lymph nodes from mice of the indicated genotypes.

(B) Representative H&E staining of spleens from compound mutant and control mice. Scale bar represents 1,000 μm; inset represents 200 μm. See a summary of histological findings in Table S1.

(C) Southern blot analysis of tumor clonality using a J_H4 probe. Dashed line represents germline *IgH* configuration. Spl, spleen; mLN, mesenteric lymph node. Clonal tumors usually exhibit two nongermline bands corresponding to *VDJ* and *DJ* rearrangements in *IgH* alleles.

(D) Immunoblot analysis of various proteins in tumor tissues from the indicated compound mutant mice or in normal spleen from a *Cγ1-cre/+* mouse. Tumor tissues, spleens of tumor-bearing mice (only those containing ~50% of lymphoma B cells, as determined by FACS analysis, were selected for this assay). β-actin serves as loading control.

(E) Representative IHC staining for IRF4/MUM1 and BCL6 on spleen sections of lymphoma-bearing compound mutants and an SRBC-immunized control mouse. Scale bar represents 1,000 μm; inset represents 200 μm. Note that BCL6 expression from the transgene is lower than that from the endogenous loci of normal GC B cells (Cattoretti et al., 2005); two *Cγ1-cre/lμBcl6* tumors are shown, and tumor #604 shows at least two populations, one of which shows relatively low IRF4 staining and high BCL6 ($IRF4^{dim}BCL6^{hi}$), while the other exhibits higher IRF4 and lower BCL6 staining ($IRF4^{hi}BCL6^{dim}$). See the summary of IHC results in Table S1.

(F) Comparison of gene expression profiles of the indicated mouse tumors to that of GC B cells (GCB), resting B cells (Resting B), or ABCs. The protein levels of IRF4 detected by IHC staining are noted next to the corresponding tumors (see also E and Table S1), which complement GEP in classification of DLBCL subtypes.

See also Figure S4 and Tables S1–S3.

(Rossi et al., 2011). Together, these observations highlight the importance of ontogenetic timing in the acquisition of oncogenic somatic mutations driving different classes of lymphomas. *TRAF3* mutations/deletions are absent in follicular lymphoma, Burkitt lymphoma, and B cell chronic lymphocytic leukemia (data not shown).

Of note, we observed that most *Cγ1-cre/lμBcl6;Nik*^{stopFL} mice developed DLBCLs of the ABC subtype. This observation is likely related to the fact that activation of the alternative NF-κB pathway interferes with the GC reaction even when BCL6 expression is deregulated and suggests that, in NF-κB positive human GCB-DLBCLs, additional mutation(s) allowing maintenance of the GCB phenotype must exist. Future studies comparing genetic lesions in the GCB versus ABC types of DLBCLs carrying *TRAF3* lesions may lead to the identification of those latter events.

Interference with Terminal B Cell Differentiation Is Required for the Pathogenesis of ABC-DLBCL: A Role for BCL6

Constitutive NF-κB signaling in B cells promotes their differentiation toward plasma cells through induction of IRF4 (Grumont and Gerondakis, 2000; Klein et al., 2006; Saito et al., 2007; Sciammas et al., 2006), in line with the presence of genetic lesions leading to constitutive NF-κB signaling in multiple myeloma (Annunziata et al., 2007; Keats et al., 2007). The observations that ABC-DLBCLs express some key genes characteristic of a plasmablast (Lenz and Staudt, 2010; Wright et al., 2003), but often carry genetic lesions interfering with plasma cell differentiation, suggest that the transformation of an ABC into DLBCL requires interference with terminal B cell differentiation (Lenz and Staudt, 2010; Staudt, 2010). Indeed, mice with specific activation of the canonical NF-κB signaling pathway in

GC B cells developed plasma cell hyperplasia and had an overall normal lifespan, but succumbed to ABC-like DLBCL when B-cell-terminal differentiation was abolished by deletion of *Blimp1* (Calado et al., 2010). Similarly, we show here that mice with activation of the alternative NF-κB pathway alone in GC B cells do not succumb to tumors in the timeframe of this study but display overt plasma cell hyperplasia and that the oncogenic role of the alternative NF-κB pathway is revealed upon interference with plasma cell differentiation through enforced BCL6 expression, in accord with the coexistence of *TRAF3* and *BCL6* mutations in human DLBCL.

Our work indicates that the role of BCL6 in the development of DLBCLs exhibiting constitutive NF-κB signaling is at least in part due to its ability to inhibit BLIMP1 expression, which in turn limits the terminal differentiation of B cells. This is supported by data showing that in the mouse loss of BLIMP1 cooperates with alternative NF-κB signaling in DLBCL formation (data not shown). However, the fact that human DLBCLs with alternative NF-κB activation are often concurrent with *BCL6* translocation but not *BLIMP1* inactivation suggests that other functions of BCL6, such as repression of the DNA damage response (Basso and Dalla-Favera, 2010), may also be critically required to complement alternative NF-κB signaling in DLBCL development.

Alternative and Canonical NF-κB Pathway Activation in DLBCLs

While mechanisms of aberrant NF-κB activation in DLBCL can in the major fraction of the cases be attributed to the presence of oncogenic mutations in genes related to the canonical NF-κB pathway (Compagno et al., 2009; Davis et al., 2010; Lenz et al., 2008; Ngo et al., 2011; Pasqualucci et al., 2011), previous data and the present work show that genetic lesions activating the alternative NF-κB pathway occur in up to 15% of DLBCLs. It is worth noting in this context that besides the ~10% DLBCL cases demonstrating nuclear NF-κB activity exclusively for the alternative pathway (indicated by nuclear staining of p52 but not p50) ~20% of DLBCLs display nuclear staining for both p50 and p52 (Compagno et al., 2009), suggesting the activation of both canonical and alternative NF-κB pathways. Indeed, our genetic analysis showed that a fraction (6 of 17) of *TRAF3*-mutated DLBCLs carries concurrent mutation(s) in genes of the canonical NF-κB pathway. Likewise, while the present mouse model suggests that the alternative pathway can by itself drive DLBCL development if combined with a lesion preventing plasma cell differentiation, it became apparent that in a small fraction (two of seven) of the resulting tumors additional mutations accumulated, which resulted in the activation of canonical NF-κB signaling. We have previously observed redundancy between the canonical and alternative NF-κB pathways to replace BAFF-mediated survival signals in B cells (Sasaki et al., 2006, 2008), and there is evidence in the human that NIK activation can also trigger canonical NF-κB activity (Annunziata et al., 2007; O'Mahony et al., 2000). Given that the NIK allele used in the present study yields only a moderate cell survival advantage, in sharp contrast to a NIK allele lacking the TRAF3 binding site (Sasaki et al., 2008), we speculate that in a NIK-expressing B cell acquisition of an activating canonical NF-κB mutation may confer a further survival advantage, enabling the cell to outcompete its siblings during the clonal evolution of lymphoma. A similar mechanism may operate in human DLBCL pathogenesis. Overall, the current work provides a rationale for the design of therapies targeting the alternative NF-κB pathway in a fraction of DLBCL patients and suggests that for those human DLBCLs that display both canonical and alternative NF-κB mutations (Compagno et al., 2009; Pasqualucci et al., 2011), targeting both arms of NF-κB signaling may be required for therapeutic intervention, as recently demonstrated for multiple myeloma (Fabre et al., 2012).

EXPERIMENTAL PROCEDURES

Sequencing Analysis and High-Density SNP Array Analysis of Human DLBCLs

One hundred nineteen DLBCL samples, including 98 biopsies (47 GCB and 51 ABC/NC-DLBCLs) and 21 cell lines (14 GCB and 7 ABC-DLBCLs), were analyzed as described previously (Pasqualucci et al., 2011). Oligonucleotides and conditions used for *TRAF3* amplification are available upon request.

Mice, Immunization, and Tumor Cohorts

Cγ1-cre, Nik^{stopFL}, $Blimp1^{FF}$, *IμBcl6*, and YFP^{stopFL} alleles have been described (Casola et al., 2006; Cattoretti et al., 2005; Ohinata et al., 2005; Sasaki et al., 2008; Srinivas et al., 2001); 8- to 10-week-old mice were immunized intravenously with 1×10^9 SRBCs (Cedarlane) in PBS. Mouse cohorts for tumor development were given monthly antigenic stimulation by SRBC immunization for seven additional times and then monitored twice a week for tumor development and euthanized if signs of tumor development occurred. All animal care and procedures followed NIH guidelines and were approved by the Institutional Animal Care and Use Committee (IACUC 03341) of Harvard University and the Immune Disease Institute.

Statistical Analysis

Unless otherwise indicated, data were analyzed using unpaired two-tailed Student's t test; a p value ≤ 0.05 was considered significant. A single asterisk (*) in the graphs of figures represents $p \leq 0.05$. Double asterisks (**) represent $p \leq 0.01$, and triple asterisks (***) represent $p \leq 0.001$; "ns" stands for not statistically significant, i.e., $p > 0.05$. Survival curves were compared using the log rank test. Data in text and figures are represented as mean ± SEM unless otherwise indicated.

ACCESSION NUMBERS

The data have been deposited to the NCBI GEO and are available under accession numbers GSE65422.

SUPPLEMENTAL INFORMATION

Supplemental Information includes Supplemental Experimental Procedures, four figures, and three tables and can be found with this article online at http://dx.doi.org/10.1016/j.celrep.2015.03.059.

AUTHOR CONTRIBUTIONS

B.Z., D.P.C., and K.R. conceived and supervised the study. B.Z., D.P.C., and Z.W. designed, performed, and analyzed the main experiments. L.P. and R.D.-F. were responsible for the human DLBCL analysis. F.W.A. supervised some aspects of the study. S.F., K.K., Y.Q., S.B.K., C.U., S.R., and W.C. performed additional experiments. M.S.-S. and Y.S. generated the NIK transgenic mice and helped conceive the study. B.Z., D.P.C., and K.R. interpreted the results and wrote the paper. All authors read and contributed to the finalization of the paper.

ACKNOWLEDGMENTS

We thank J. Xia, X. Chen, D. Ghitza, A. Pellerin, J. Grundy, and C. Langnick for technical assistance; M. Bamberg, M. Ottaviano, H.-L. Cheng, J. Needham, and L. Lynch for administrative assistance; and K.R. laboratory members and M. Janz for critical comments and suggestions. This work was supported by the National Cancer Institute grants P01 CA092625 and R01 CA098285, a Leukemia & Lymphoma Society SCOR grant, and the European Research Council, ERC Advanced Grant ERC-AG-LS6 to K.R.; the National Cancer Institute grant CA172492 to L.P.; the Leukemia & Lymphoma Society fellowships to B.Z. and D.P.C.; the Dana-Farber Cancer Institute Faculty Startup Funds to B.Z.; and core funding from Cancer Research UK, and a MRC career development award MR/J008060/1 to D.C.

Received: April 24, 2014
Revised: January 29, 2015
Accepted: March 24, 2015
Published: April 23, 2015

REFERENCES

Alizadeh, A.A., Eisen, M.B., Davis, R.E., Ma, C., Lossos, I.S., Rosenwald, A., Boldrick, J.C., Sabet, H., Tran, T., Yu, X., et al. (2000). Distinct types of diffuse large B-cell lymphoma identified by gene expression profiling. Nature *403*, 503–511.

Annunziata, C.M., Davis, R.E., Demchenko, Y., Bellamy, W., Gabrea, A., Zhan, F., Lenz, G., Hanamura, I., Wright, G., Xiao, W., et al. (2007). Frequent engagement of the classical and alternative NF-kappaB pathways by diverse genetic abnormalities in multiple myeloma. Cancer Cell *12*, 115–130.

Basso, K., and Dalla-Favera, R. (2010). BCL6: master regulator of the germinal center reaction and key oncogene in B cell lymphomagenesis. Adv. Immunol. *105*, 193–210.

Bidère, N., Ngo, V.N., Lee, J., Collins, C., Zheng, L., Wan, F., Davis, R.E., Lenz, G., Anderson, D.E., Arnoult, D., et al. (2009). Casein kinase 1alpha governs antigen-receptor-induced NF-kappaB activation and human lymphoma cell survival. Nature *458*, 92–96.

Brown, K., Gerstberger, S., Carlson, L., Franzoso, G., and Siebenlist, U. (1995). Control of I kappa B-alpha proteolysis by site-specific, signal-induced phosphorylation. Science *267*, 1485–1488.

Calado, D.P., Zhang, B., Srinivasan, L., Sasaki, Y., Seagal, J., Unitt, C., Rodig, S., Kutok, J., Tarakhovsky, A., Schmidt-Supprian, M., and Rajewsky, K. (2010). Constitutive canonical NF-κB activation cooperates with disruption of BLIMP1 in the pathogenesis of activated B cell-like diffuse large cell lymphoma. Cancer Cell *18*, 580–589.

Casola, S., Cattoretti, G., Uyttersprot, N., Koralov, S.B., Seagal, J., Hao, Z., Waisman, A., Egert, A., Ghitza, D., and Rajewsky, K. (2006). Tracking germinal center B cells expressing germ-line immunoglobulin gamma1 transcripts by conditional gene targeting. Proc. Natl. Acad. Sci. USA *103*, 7396–7401.

Cattoretti, G., Pasqualucci, L., Ballon, G., Tam, W., Nandula, S.V., Shen, Q., Mo, T., Murty, V.V., and Dalla-Favera, R. (2005). Deregulated BCL6 expression recapitulates the pathogenesis of human diffuse large B cell lymphomas in mice. Cancer Cell *7*, 445–455.

Choi, W.W., Weisenburger, D.D., Greiner, T.C., Piris, M.A., Banham, A.H., Delabie, J., Braziel, R.M., Geng, H., Iqbal, J., Lenz, G., et al. (2009). A new immunostain algorithm classifies diffuse large B-cell lymphoma into molecular subtypes with high accuracy. Clin. Cancer Res. *15*, 5494–5502.

Compagno, M., Lim, W.K., Grunn, A., Nandula, S.V., Brahmachary, M., Shen, Q., Bertoni, F., Ponzoni, M., Scandurra, M., Califano, A., et al. (2009). Mutations of multiple genes cause deregulation of NF-kappaB in diffuse large B-cell lymphoma. Nature *459*, 717–721.

Davis, R.E., Brown, K.D., Siebenlist, U., and Staudt, L.M. (2001). Constitutive nuclear factor kappaB activity is required for survival of activated B cell-like diffuse large B cell lymphoma cells. J. Exp. Med. *194*, 1861–1874.

Davis, R.E., Ngo, V.N., Lenz, G., Tolar, P., Young, R.M., Romesser, P.B., Kohlhammer, H., Lamy, L., Zhao, H., Yang, Y., et al. (2010). Chronic active B-cell-receptor signalling in diffuse large B-cell lymphoma. Nature *463*, 88–92.

Fabre, C., Mimura, N., Bobb, K., Kong, S.Y., Gorgun, G., Cirstea, D., Hu, Y., Minami, J., Ohguchi, H., Zhang, J., et al. (2012). Dual inhibition of canonical and noncanonical NF-κB pathways demonstrates significant antitumor activities in multiple myeloma. Clin. Cancer Res. *18*, 4669–4681.

Gardam, S., Sierro, F., Basten, A., Mackay, F., and Brink, R. (2008). TRAF2 and TRAF3 signal adapters act cooperatively to control the maturation and survival signals delivered to B cells by the BAFF receptor. Immunity *28*, 391–401.

Grumont, R.J., and Gerondakis, S. (2000). Rel induces interferon regulatory factor 4 (IRF-4) expression in lymphocytes: modulation of interferon-regulated gene expression by rel/nuclear factor kappaB. J. Exp. Med. *191*, 1281–1292.

Häcker, H., Tseng, P.H., and Karin, M. (2011). Expanding TRAF function: TRAF3 as a tri-faced immune regulator. Nat. Rev. Immunol. *11*, 457–468.

Hans, C.P., Weisenburger, D.D., Greiner, T.C., Gascoyne, R.D., Delabie, J., Ott, G., Müller-Hermelink, H.K., Campo, E., Braziel, R.M., Jaffe, E.S., et al. (2004). Confirmation of the molecular classification of diffuse large B-cell lymphoma by immunohistochemistry using a tissue microarray. Blood *103*, 275–282.

He, J.Q., Saha, S.K., Kang, J.R., Zarnegar, B., and Cheng, G. (2007). Specificity of TRAF3 in its negative regulation of the noncanonical NF-kappa B pathway. J. Biol. Chem. *282*, 3688–3694.

Iqbal, J., Greiner, T.C., Patel, K., Dave, B.J., Smith, L., Ji, J., Wright, G., Sanger, W.G., Pickering, D.L., Jain, S., et al.; Leukemia/Lymphoma Molecular Profiling Project (2007). Distinctive patterns of BCL6 molecular alterations and their functional consequences in different subgroups of diffuse large B-cell lymphoma. Leukemia *21*, 2332–2343.

Kato, M., Sanada, M., Kato, I., Sato, Y., Takita, J., Takeuchi, K., Niwa, A., Chen, Y., Nakazaki, K., Nomoto, J., et al. (2009). Frequent inactivation of A20 in B-cell lymphomas. Nature *459*, 712–716.

Keats, J.J., Fonseca, R., Chesi, M., Schop, R., Baker, A., Chng, W.J., Van Wier, S., Tiedemann, R., Shi, C.X., Sebag, M., et al. (2007). Promiscuous mutations activate the noncanonical NF-kappaB pathway in multiple myeloma. Cancer Cell *12*, 131–144.

Klein, U., Casola, S., Cattoretti, G., Shen, Q., Lia, M., Mo, T., Ludwig, T., Rajewsky, K., and Dalla-Favera, R. (2006). Transcription factor IRF4 controls plasma cell differentiation and class-switch recombination. Nat. Immunol. *7*, 773–782.

Lenz, G., and Staudt, L.M. (2010). Aggressive lymphomas. N. Engl. J. Med. *362*, 1417–1429.

Lenz, G., Davis, R.E., Ngo, V.N., Lam, L., George, T.C., Wright, G.W., Dave, S.S., Zhao, H., Xu, W., Rosenwald, A., et al. (2008). Oncogenic CARD11 mutations in human diffuse large B cell lymphoma. Science *319*, 1676–1679.

Mandelbaum, J., Bhagat, G., Tang, H., Mo, T., Brahmachary, M., Shen, Q., Chadburn, A., Rajewsky, K., Tarakhovsky, A., Pasqualucci, L., and Dalla-Favera, R. (2010). BLIMP1 is a tumor suppressor gene frequently disrupted in activated B cell-like diffuse large B cell lymphoma. Cancer Cell *18*, 568–579.

Martins, G., and Calame, K. (2008). Regulation and functions of Blimp-1 in T and B lymphocytes. Annu. Rev. Immunol. *26*, 133–169.

Monti, S., Savage, K.J., Kutok, J.L., Feuerhake, F., Kurtin, P., Mihm, M., Wu, B., Pasqualucci, L., Neuberg, D., Aguiar, R.C., et al. (2005). Molecular profiling of diffuse large B-cell lymphoma identifies robust subtypes including one characterized by host inflammatory response. Blood *105*, 1851–1861.

Moore, C.R., Liu, Y., Shao, C., Covey, L.R., Morse, H.C., 3rd, and Xie, P. (2012). Specific deletion of TRAF3 in B lymphocytes leads to B-lymphoma development in mice. Leukemia *26*, 1122–1127.

Morin, R.D., Mendez-Lago, M., Mungall, A.J., Goya, R., Mungall, K.L., Corbett, R.D., Johnson, N.A., Severson, T.M., Chiu, R., Field, M., et al. (2011). Frequent mutation of histone-modifying genes in non-Hodgkin lymphoma. Nature *476*, 298–303.

Neri, A., Chang, C.C., Lombardi, L., Salina, M., Corradini, P., Maiolo, A.T., Chaganti, R.S., and Dalla-Favera, R. (1991). B cell lymphoma-associated

chromosomal translocation involves candidate oncogene lyt-10, homologous to NF-kappa B p50. Cell *67*, 1075–1087.

Ngo, V.N., Young, R.M., Schmitz, R., Jhavar, S., Xiao, W., Lim, K.H., Kohlhammer, H., Xu, W., Yang, Y., Zhao, H., et al. (2011). Oncogenically active MYD88 mutations in human lymphoma. Nature *470*, 115–119.

O'Mahony, A., Lin, X., Geleziunas, R., and Greene, W.C. (2000). Activation of the heterodimeric IkappaB kinase alpha (IKKalpha)-IKKbeta complex is directional: IKKalpha regulates IKKbeta under both basal and stimulated conditions. Mol. Cell. Biol. *20*, 1170–1178.

Ohinata, Y., Payer, B., O'Carroll, D., Ancelin, K., Ono, Y., Sano, M., Barton, S.C., Obukhanych, T., Nussenzweig, M., Tarakhovsky, A., et al. (2005). Blimp1 is a critical determinant of the germ cell lineage in mice. Nature *436*, 207–213.

Pasqualucci, L., Compagno, M., Houldsworth, J., Monti, S., Grunn, A., Nandula, S.V., Aster, J.C., Murty, V.V., Shipp, M.A., and Dalla-Favera, R. (2006). Inactivation of the PRDM1/BLIMP1 gene in diffuse large B cell lymphoma. J. Exp. Med. *203*, 311–317.

Pasqualucci, L., Trifonov, V., Fabbri, G., Ma, J., Rossi, D., Chiarenza, A., Wells, V.A., Grunn, A., Messina, M., Elliot, O., et al. (2011). Analysis of the coding genome of diffuse large B-cell lymphoma. Nat. Genet. *43*, 830–837.

Pham, L.V., Fu, L., Tamayo, A.T., Bueso-Ramos, C., Drakos, E., Vega, F., Medeiros, L.J., and Ford, R.J. (2011). Constitutive BR3 receptor signaling in diffuse, large B-cell lymphomas stabilizes nuclear factor-κB-inducing kinase while activating both canonical and alternative nuclear factor-κB pathways. Blood *117*, 200–210.

Rossi, D., Deaglio, S., Dominguez-Sola, D., Rasi, S., Vaisitti, T., Agostinelli, C., Spina, V., Bruscaggin, A., Monti, S., Cerri, M., et al. (2011). Alteration of BIRC3 and multiple other NF-κB pathway genes in splenic marginal zone lymphoma. Blood *118*, 4930–4934.

Saito, M., Gao, J., Basso, K., Kitagawa, Y., Smith, P.M., Bhagat, G., Pernis, A., Pasqualucci, L., and Dalla-Favera, R. (2007). A signaling pathway mediating downregulation of BCL6 in germinal center B cells is blocked by BCL6 gene alterations in B cell lymphoma. Cancer Cell *12*, 280–292.

Sasaki, Y., Derudder, E., Hobeika, E., Pelanda, R., Reth, M., Rajewsky, K., and Schmidt-Supprian, M. (2006). Canonical NF-kappaB activity, dispensable for B cell development, replaces BAFF-receptor signals and promotes B cell proliferation upon activation. Immunity *24*, 729–739.

Sasaki, Y., Calado, D.P., Derudder, E., Zhang, B., Shimizu, Y., Mackay, F., Nishikawa, S., Rajewsky, K., and Schmidt-Supprian, M. (2008). NIK overexpression amplifies, whereas ablation of its TRAF3-binding domain replaces BAFF:BAFF-R-mediated survival signals in B cells. Proc. Natl. Acad. Sci. USA *105*, 10883–10888.

Sciammas, R., Shaffer, A.L., Schatz, J.H., Zhao, H., Staudt, L.M., and Singh, H. (2006). Graded expression of interferon regulatory factor-4 coordinates isotype switching with plasma cell differentiation. Immunity *25*, 225–236.

Shaffer, A.L., 3rd, Young, R.M., and Staudt, L.M. (2012). Pathogenesis of human B cell lymphomas. Annu. Rev. Immunol. *30*, 565–610.

Srinivas, S., Watanabe, T., Lin, C.S., William, C.M., Tanabe, Y., Jessell, T.M., and Costantini, F. (2001). Cre reporter strains produced by targeted insertion of EYFP and ECFP into the ROSA26 locus. BMC Dev. Biol. *1*, 4.

Staudt, L.M. (2010). Oncogenic activation of NF-kappaB. Cold Spring Harb. Perspect. Biol. *2*, a000109.

Tam, W., Gomez, M., Chadburn, A., Lee, J.W., Chan, W.C., and Knowles, D.M. (2006). Mutational analysis of PRDM1 indicates a tumor-suppressor role in diffuse large B-cell lymphomas. Blood *107*, 4090–4100.

Traenckner, E.B., Pahl, H.L., Henkel, T., Schmidt, K.N., Wilk, S., and Baeuerle, P.A. (1995). Phosphorylation of human I kappa B-alpha on serines 32 and 36 controls I kappa B-alpha proteolysis and NF-kappa B activation in response to diverse stimuli. EMBO J. *14*, 2876–2883.

Tunyaplin, C., Shaffer, A.L., Angelin-Duclos, C.D., Yu, X., Staudt, L.M., and Calame, K.L. (2004). Direct repression of prdm1 by Bcl-6 inhibits plasmacytic differentiation. J. Immunol. *173*, 1158–1165.

Wright, G., Tan, B., Rosenwald, A., Hurt, E.H., Wiestner, A., and Staudt, L.M. (2003). A gene expression-based method to diagnose clinically distinct subgroups of diffuse large B cell lymphoma. Proc. Natl. Acad. Sci. USA *100*, 9991–9996.

Ye, B.H., Cattoretti, G., Shen, Q., Zhang, J., Hawe, N., de Waard, R., Leung, C., Nouri-Shirazi, M., Orazi, A., Chaganti, R.S., et al. (1997). The BCL-6 proto-oncogene controls germinal-centre formation and Th2-type inflammation. Nat. Genet. *16*, 161–170.

Cell Reports

Supplemental Information

An Oncogenic Role for Alternative NF-κB Signaling in DLBCL Revealed upon Deregulated BCL6 Expression

Baochun Zhang, Dinis Pedro Calado, Zhe Wang, Sebastian Fröhler, Karl Köchert, Yu Qian, Sergei B. Koralov, Marc Schmidt-Supprian, Yoshiteru Sasaki, Christine Unitt, Scott Rodig, Wei Chen, Riccardo Dalla-Favera, Frederick W. Alt, Laura Pasqualucci, and Klaus Rajewsky

SUPPLEMENTAL INFORMATION

Inventory of Supplemental Information

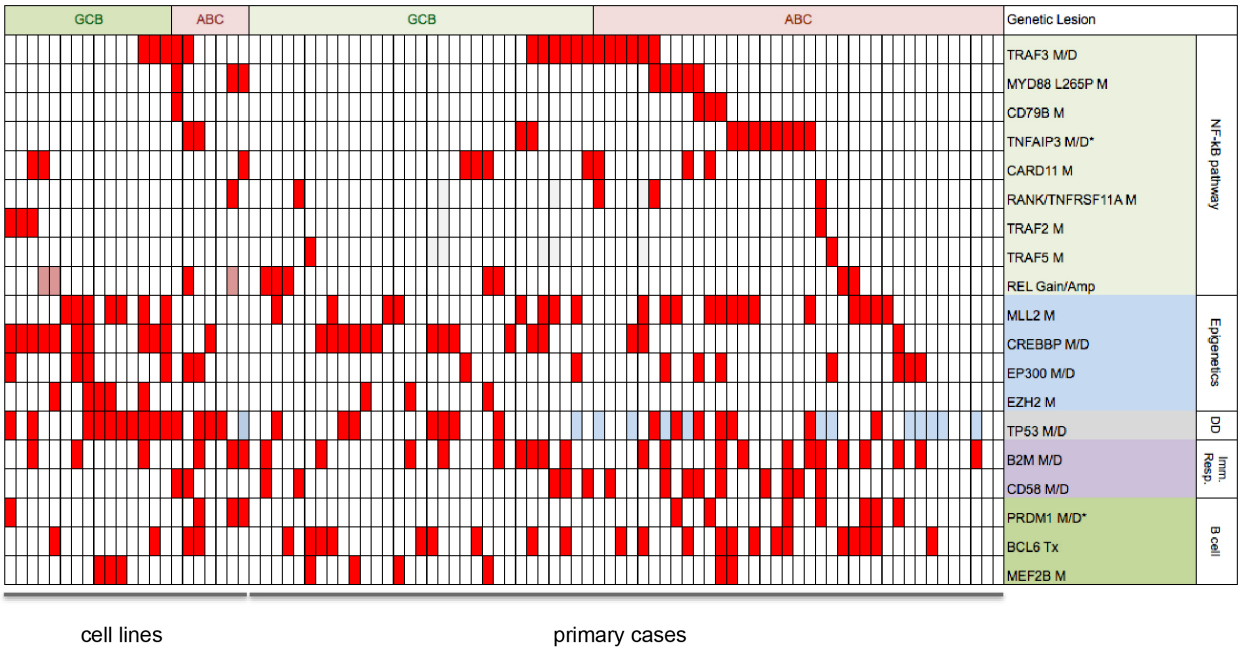

Figure S1. Relationship between *TRAF3* Genetic Lesions and Other Recurrent Alterations in DLBCL, Related to Figure 1

Relative distribution of recurrent genetic lesions in DLBCL cell lines and patient biopsies; Columns represent individual samples and rows correspond to distinct genetic lesions, grouped into separate functional categories (M, mutation, D, deletion, Tx, translocation, Amp, high copy number amplification; DD, DNA damage response). Red and white colors denote the presence or absence of the lesion, respectively; light red in *REL* indicates low copy number gains; light blue in *TP53* identifies monoallelic deletions, the pathogenic significance of which is unclear. *, for these genes only biallelic alterations are shown.

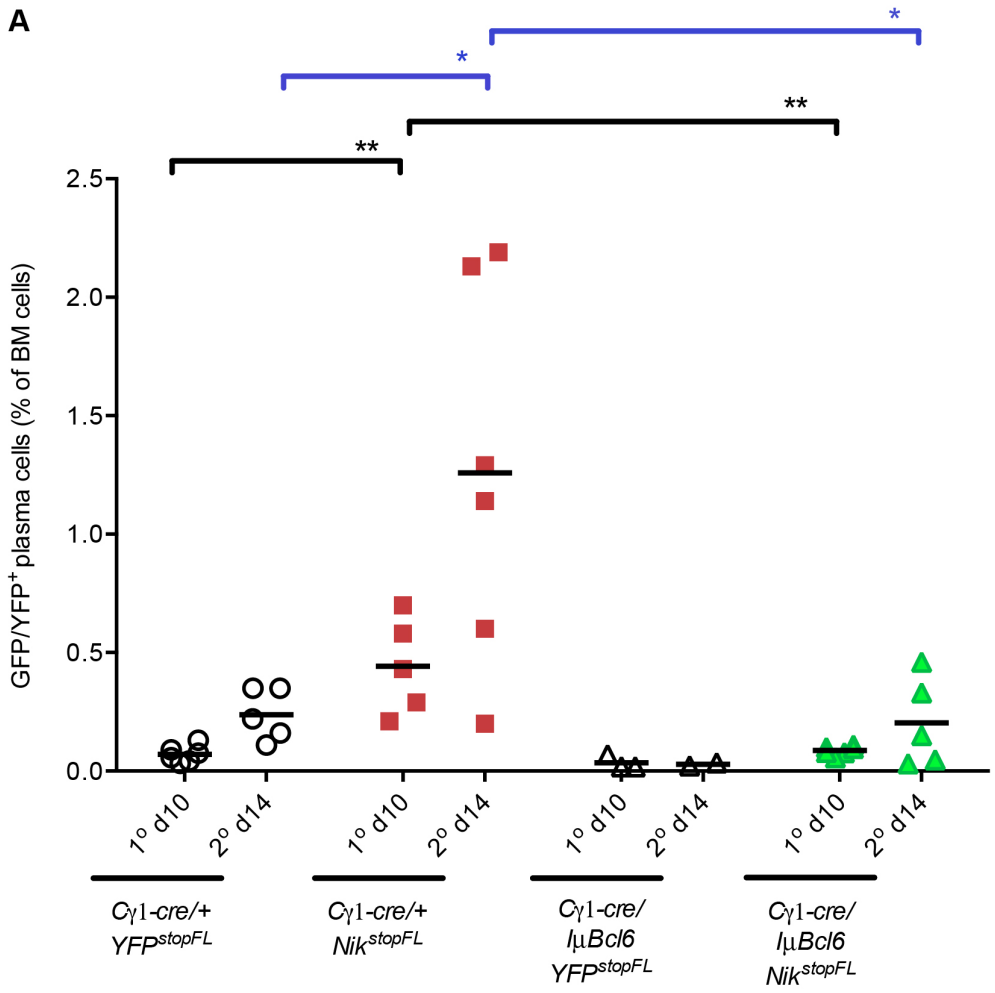
A
*
*
**
**
GFP/YFP+ plasma cells (% of BM cells)
2.5
2.0
1.5
1.0
0.5
0.0
1° d10
2° d14
1° d10
2° d14
1° d10
2° d14
1° d10
2° d14
Cγ1-cre/+
YFPstopFL
Cγ1-cre/+
Nikstop FL
Cγ1-cre/
IμBcl6
YFPstopFL
Cγ1-cre/
IμBcl6
Nikstop FL

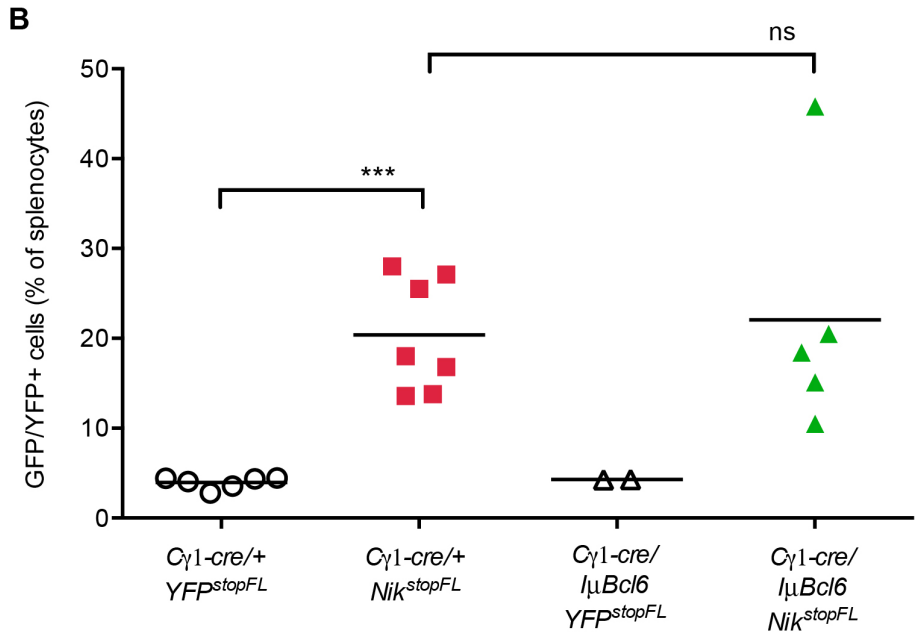
B
ns
***
GFP/YFP+ cells (% of splenocytes)
50
40
30
20
10
0
Cγ1-cre/+
YFPstopFL
Cγ1-cre/+
Nikstop FL
Cγ1-cre/
IμBcl6
YFPstopFL
Cγ1-cre/
IμBcl6
Nikstop FL

Figure S2. Constitutive BCL6 Expression Represses NIK-induced Plasma Cell Differentiation, Related to Figure 4

(A) Summary of FACS analysis of reporter positive plasma cells in bone marrow (BM) at day 10 after primary immunization and day 14 after secondary immunization. Black bar represents mean.

(B) Summary of FACS analysis of reporter positive cells in spleen of the indicated mice at day 14 after secondary immunization. Black bar represents mean.

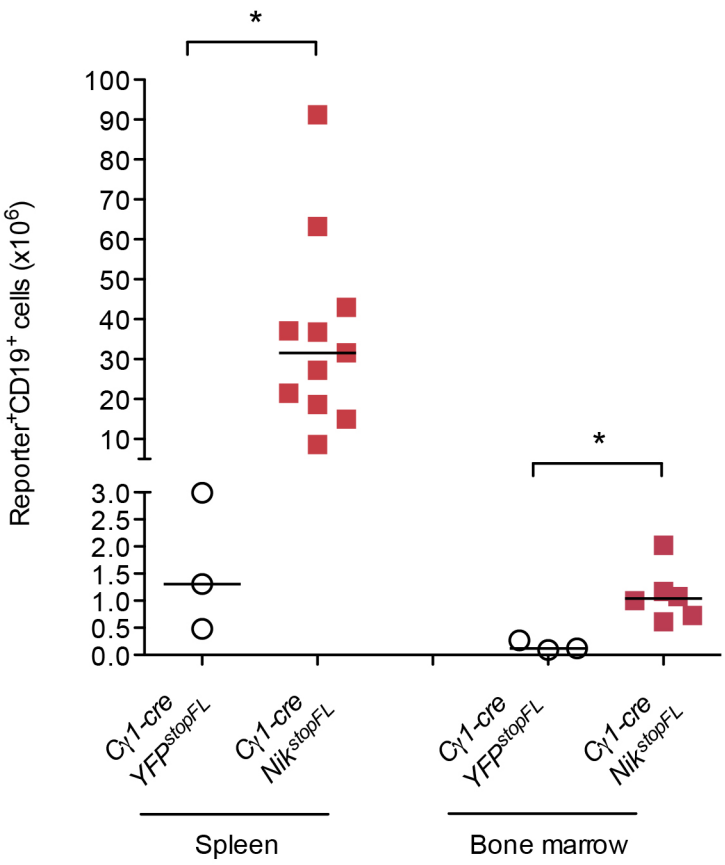

Figure S3. Constitutive Alternative NF-κB Signaling Promotes B Cell Hyperplasia, Related to Figure 6

Summary of FACS analysis of reporter positive, $CD19^+$ B cells in spleen and bone marrow of aged (≥ 60 weeks) mice of the indicated genotypes. Black bar represents median. The statistics was analyzed using unpaired, nonparametric Mann-Whitney test.

A

Gene	Tumor	Genotype	DLBCL subtype	Amino acid change due to nucleotide mutation	Frequency of transcript reads
CARD11	603	*Cγ1-cre/IμBcl6*	GCB	D401N	59.44%
CSNK1A1 (CK1α)	1128	*Cγ1-cre/IμBcl6*	ABC	A44V	41.74%
MYD88	773	*Cγ1-cre/IμBcl6;Nik^{stopFL}*	ABC	R218H	64.42%
	776	*Cγ1-cre/IμBcl6;Nik^{stopFL}*	ABC	R218H	41.77%

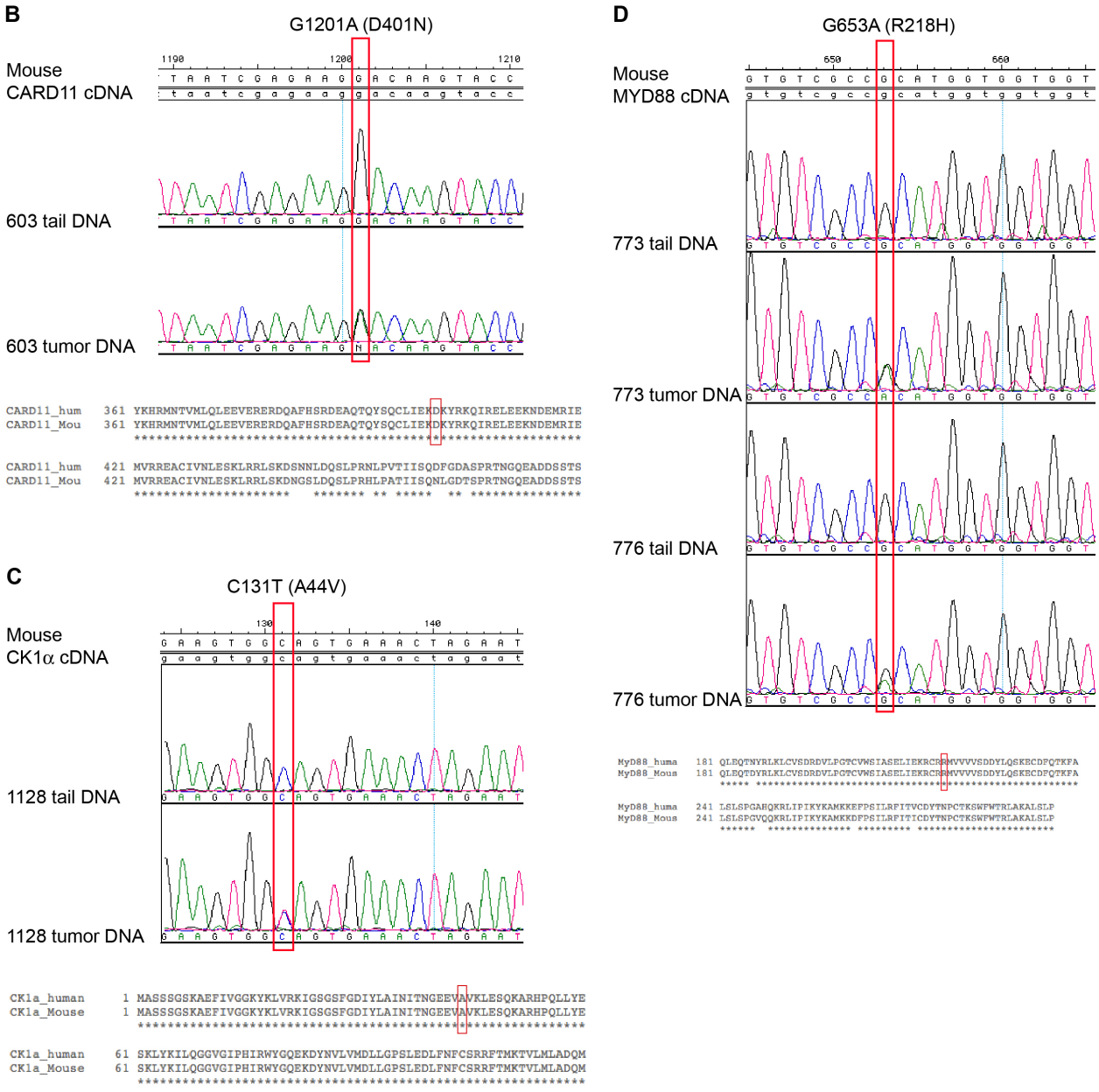

Figure S4. RNA Sequencing in the Mouse Tumors Identifies Somatic Mutation of Genes Involved in Canonical NF-κB Signaling, Related to Figure 7

(A) Non-silent Mutations identified by RNA sequencing in the indicated tumors, which were subsequently confirmed by Sanger sequencing.

(B-D) Confirmation of somatic origin of the mutations by analysis of paired normal (tail) DNA. Sanger sequencing of the indicated genomic regions of *CARD11* (B), *CK1a* (C) and *MYD88* (D) in mouse tumors and the corresponding tails was aligned to the coding sequence (cDNA) of each gene. The nucleotide changes and the predicted amino acid changes (in parentheses) are given at the top of each figure. Shown at the bottom of each figure is the alignment of the indicated protein sequence in the human and mouse, with the mutation position denoted by a red rectangle.

Table S1. Histology and Immunohistochemistry of the Tumors, Related to Figure 7

Genotype	Mice	Organ	Histology	IHC	
				IRF4	BCL6
Cγ1cre/ IμBcl6; Nik^{stopFL}	611	Spleen	DLBCL		
		mLN	DLBCL		
	773	Spleen	DLBCL		
		mLN	DLBCL		
	776	Spleen	DLBCL	hi	dim
		mLN	DLBCL		
		tLN	DLBCL		
	817	Spleen	DLBCL		
		mLN	DLBCL		
		tLN	DLBCL		
	818	Spleen	DLBCL	hi	dim
		mLN	DLBCL		
	920	Spleen	DLBCL	hi	dim
		mLN	DLBCL		
	1078	Spleen	DLBCL	hi	dim
		mLN	DLBCL		
	1110	Spleen	DLBCL	hi	dim
		mLN	DLBCL		
Cγ1cre/ IμBcl6	603	Spleen	DLBCL		
		mLN	DLBCL		
	604	Spleen	DLBCL	dim/hi ¶	hi/dim
	607	Spleen	DLBCL	hi	dim
		mLN	DLBCL		
	775	Spleen	DLBCL		
		mLN	DLBCL		
	857	Spleen	Plasmacytic	lo/neg	dim
	1128	Spleen	DLBCL	hi	dim
		mLN	DLBCL		

¶This tumor contains at least two populations, one of which is IRF4^{dim}BCL6^{hi} while the other is IRF4^{hi}BCL6^{dim}. See also Figure 7. Hi, high; lo/neg, low/negative.

Table S2. Surface Phenotype of Tumor Cells, Related to Figure 7

Cγ1-cre/IμBcl6	
Mice	Surface phenotype
603	CD19+, IgM+, Igκ+, CD38^{hi}, AA4.1-, CD21^{lo}, CD23^{lo}, CD138-, CD43-
604	CD19+, IgM+, Igκ+, CD38^{hi}, AA4.1-, CD21^{lo}, CD23^{lo}, CD138-, CD43^{int}
607	CD19+, IgM+, Igκ+, CD38^{hi}, AA4.1-, CD21^{lo}, CD23^{lo}, CD138-, CD43^{int}
775	CD19+, IgG2+, Igκ+, CD38^{hi}, AA4.1-, CD21^{lo}, CD23^{lo}, CD138-, CD43-
857	N.D.
1128	CD19+, IgM+, CD38+, AA4.1-, CD21^{lo}, CD23^{lo}, CD138-, CD43-
Cγ1-cre/IμBcl6;Nik^{stopFL}	
Mice	Surface phenotype
611	CD19+, IgM+, Igκ+, CD38+, AA4.1-, CD21^{lo}, CD23^{lo}, CD138-, CD43-
773	CD19+, IgM+, Igκ+, CD38^{hi}, AA4.1-, CD21^{lo}, CD23^{lo}, CD138-, CD43^{int}
776	CD19+, IgM+, Igκ+, CD38^{hi}, AA4.1-, CD21^{lo}, CD23^{lo}, CD138-, CD43-
817	CD19+, IgM+, Igκ+, CD38^{hi}, AA4.1-, CD21^{lo}, CD23^{lo}, CD138-, CD43-
818	CD19+, IgG3+, Igκ+, CD38^{hi}, AA4.1-, CD21^{lo}, CD23^{lo}, CD138-, CD43-
920	CD19+, IgM+, CD38^{hi}, AA4.1-, CD21^{lo}, CD23^{lo}, CD138-, CD43-
1078	CD19+, IgM+, CD38+, AA4.1-, CD21^{lo}, CD23^{lo}, CD138-, CD43+
1110	CD19+, IgM+, CD38+, AA4.1-, CD21^{lo}, CD23^{lo}, CD138-, CD43-

Abbreviations: hi, high; lo, low; int, intermediate; N.D., not done.

Table S3. SHM Analysis of Tumor Samples, Related to Figure 7

Genotype/Mice	V_H	D_H	J_H	Nucleotides analyzed (#)	Mutations (#)	Frequency of mutation (%)
Cγ1-cre/IμBcl6;Nik^{stopFL}						
#611	*VH7183.a2.3*	*DST4*	*JH4*	560	1	0.18
#817	*J558.33*	*DFL16.1*	*JH2*	380	3	0.79
#920	*J558.45*	*DQ52*	*JH2*	380	0	0
#1078	*J558.19.109*	*DFL16.1*	*JH1*	320	0	0
Cγ1-cre/IμBcl6						
#603	*J558.35*	*DSP2.8*	*JH3*	530	3	0.57
#604	*VH7183.a47.76*	*DSP2.12*	*JH3*	480	5	1.04
#607	*J558.n*	*DSP2.2*	*JH3*	530	1	0.19
#1128	*VH105*	*DSP2.7*	*JH4*	560	0	0

SUPPLEMENTAL EXPERIMENTAL PROCEDURES

Flow Cytometry

Single cell suspensions prepared from various lymphoid organs were stained with the following antibodies: anti-CD19 (1D3), -B220 (RA3-6B2), -CD138 (281-2), -Fas (Jo2), -CD43 (S7), -Igκ (187.1), -IgG2a/2b (R2-40), -IgG3 (R40-82) (all from BD); anti-CD93 (AA4.1), -CD38 (90) (eBioscience); anti-CD21 (7E9), -CD23 (B3B4) (Biolegend); anti-IgM (Fab fragment, Jackson Immunoresearch). Samples were acquired on a FACSCanto II (BD), and analyzed using FlowJo software (Tree Star).

Real-Time RT-PCR

Total RNA was extracted using TRIzol reagent, and cDNA was synthesized using the ThermoScript RT-PCR System (Invitrogen). For qRT-PCR we used Power SYBR Green, followed by analysis with the StepOnePlus System (Applied Biosystems). Samples were assayed in triplicate, and values normalized to HPRT levels.

Primer sequences:

Bcl6	5′-GCCCACGTTCCCGGAGGAGA-3′
	5′-CGTCTGCAGCGTGTGCCTCT-3′
Irf4	5′-AGGTCTGCTGAAGCCTTGGC-3′
	5′-CTTCAGGGCTCGTCGTGGTC-3′
Blimp1	5′-GGCTCCACTACCCTTATCCTGGAGG-3′
	5′-ACGCTGTACTCTCTCTTGGGGACAC-3′
Aicda	5′-TAGTGCCACCTCCTGCTCACT-3′
	5′-CAACAATTCCACGTGGCAGCC-3′
Hprt	5′-GTCATGCCGACCCGCAGTC-3′
	5′-GTCCTGTCCATAATCAGTCCATGAGGAATAAAC-3′

Cell Culture, Apoptosis and Proliferation Assays

Splenic B cells were purified by CD43-depletion (Miltenyi). Cells were cultured in the presence of 1 μg/ml anti-CD40 (HM40-3; eBioscience) and 25 ng/ml IL-4 (R&D Systems). To monitor cellular division, B cells were labeled with CellTrace™ Violet (Invitrogen) per the manufacturer's instructions. Cells undergoing apoptosis were detected using the Active Caspase-3 Apoptosis Kit (BD), according to manufacturer's instructions.

Histology and Immunohistochemistry

For histological examination, tissues were fixed with 10% formalin (Sigma), embedded in paraffin, sectioned at 5 μm and stained with hematoxylin and eosin (H&E). Immunohistochemical staining was performed with anti-IRF4 (MUM1; Santa Cruz), anti-BCL6 (D65C10; Cell Signaling Technology), anti-CD138 (281-2; BD), and anti-mouse Ig (Vector).

Immunoblot Analysis

Protein extracts were fractionated on 10% sodium dodecyl sulfate polyacrylamide gels, transferred onto polyvinylidene difluoride membranes, and immunoblotted with the following primary antibodies: anti-NF-κB2 p100 (#4882), anti-phospho-IκBα (#9246), anti-BCL6 (#5650) (all from Cell Signaling Technology); anti-IκBα (SC-371, Santa Cruz), and anti-β-Actin (A5316, Sigma).

Serum Protein Electrophoresis

Serum was diluted 1:2 in barbital buffer and analyzed on a Hydragel K20 system

according to manufacturer's instruction (Sebia).

Analysis of Tumor Clonality

The clonality of lymphomas was determined by Southern blotting of EcoRI-digested genomic DNA from tumors using a J_H probe spanning the *J_H4* exon and part of the downstream intronic sequence.

***IgH* Somatic Mutation Analysis**

Genomic DNA was prepared from tumor tissues or sorted GC B cells. *IgH-V* gene rearrangements were PCR amplified using the Expand High Fidelity PCR System (Roche) with forward primers V_HA and V_HE adapted from (Ehlich et al., 1994) and a reverse primer in the *J_H4* intron (5'-CTCCACCAGACCTCTCTAGACAGC-3'). Fragments were cloned, sequenced, and blasted against the NCBI database (http://www.ncbi.nlm.nih.gov/igblast/) to determine *$V_HD_HJ_H$* usage. The cloned intronic sequences were then aligned to their germline counterparts. In determining somatic mutations we excluded polymorphisms associated with the *Cγ1-cre* allele.

RNA Sequencing and Analysis

Illumina TrueSeq mRNA-seq libraries were prepared from total RNA according to the manufacturer's instructions (Illumina). All libraries were sequenced in 6-plex pools, two lanes per pool, for 1x101 cycles on an Illumina HiSeq2000 instrument. An average of 65,061,816 single-end 101bp reads were generated per sample, of which ~93.37% on average could be mapped onto the ENSEMBL NCBIM37.67 mouse reference genome

sequence using TopHat (Trapnell et al., 2009). An average of 72.59% of all mapped bases per sample were aligned within ENSEMBL gene bodies. For expression analysis, reads uniquely mapping to individual ENSEMBL genes were counted using htseq-count (http://www-huber.embl.de/users/anders/HTSeq). Gene expression was quantified using edgeR based on a negative binomial generalized log-linear model (Robinson et al., 2010). Biological reproducibility between the replicates was excellent (Pearson correlation: 0.990899). For classification of the mouse DLBCLs, hierarchical clustering was applied based on the expression of all genes. Euclidean distance and complete linkage was used to assess the similarity between individual DLBCL samples and GC B cells (GCB), resting B cells (Resting B), or *in vitro* activated B cells (ABC) prepared using anti-CD40 and anti-IgM antibodies. Sequence variants were detected within the mRNA-seq reads using VarScan (Koboldt et al., 2009). A minimum coverage of 10 uniquely mapping reads in each sample was required in order to call a variant. Variants with alternative allele frequencies between 8% and 75% were defined as being heterozygous. Sequence variants were annotated with their predicted effect on protein coding sequence using snpEff (PMID: 22728672) based on ENSEMBL NCBIM37.67 gene models. Somatic variants and loss-of-heterozygosity events were extracted from the total list of variants by comparing each tumor sample to the resting B-cell control samples. The VarScan probability of a variant to be somatic was thresholded at a 5% false-positive rate.

List of NF-κB Related Genes Analyzed for Mutation in the Mouse Tumors

BCL10, BIRC2 (cIAP1), BIRC3 (cIAP2), CARD11, CD40, CHUK (IKKα), CSNK1A1, CYLD, IKBKB (IKKβ), IKBKG (NEMO), Tnfrsf11a (Rank), MALT1, MAP3K14 (NIK), MAP3K7 (TAK1), MAP3K7IP2 (TAB2), MAP3K7IP3 (TAB3), NFKB1 (p105/p50), NFKBIA (IκBα), NFKBIB (IκBβ), PRKCB1, REL (cREL), TNFAIP3 (A20), TNFRSF11A (RANK), TNFRSF13C (BAFFR), TNFSF13B (BAFF), TRAF1, TRAF2, TRAF3, TRAF4, TRAF5, TRAF6, TBK1, MYD88, CD79b

SUPPLEMENTAL REFERENCES

Ehlich, A., Martin, V., Muller, W., and Rajewsky, K. (1994). Analysis of the B-cell progenitor compartment at the level of single cells. Current biology : CB *4*, 573-583.

Koboldt, D.C., Chen, K., Wylie, T., Larson, D.E., McLellan, M.D., Mardis, E.R., Weinstock, G.M., Wilson, R.K., and Ding, L. (2009). VarScan: variant detection in massively parallel sequencing of individual and pooled samples. Bioinformatics *25*, 2283-2285.

Robinson, M.D., McCarthy, D.J., and Smyth, G.K. (2010). edgeR: a Bioconductor package for differential expression analysis of digital gene expression data. Bioinformatics *26*, 139-140.

Trapnell, C., Pachter, L., and Salzberg, S.L. (2009). TopHat: discovering splice junctions with RNA-Seq. Bioinformatics *25*, 1105-1111.